Regular Research Article
Short Title: Frequency response of photosynthesis
Author for Contact: Ladislav Nedbal, l.nedbal@fz-juelich.de

Photosynthesis dynamics and regulation sensed in the frequency domain

Ladislav Nedbal[1] and Dušan Lazár[2]

[1] Institute of Bio- and Geosciences/Plant Sciences (IBG-2), Forschungszentrum Jülich, Wilhelm-Johnen-Straße, D-52428 Jülich, Germany

[2] Department of Biophysics, Centre of the Region Haná for Biotechnological and Agricultural Research, Šlechtitelů 27, 783 71 Olomouc, Czech Republic

One sentence summary: It is proposed to characterize photosynthesis in the frequency domain without the need for dark adaptation and, thus, without assumptions about the dark-to-light transition.

Funding information:
L.N. gratefully acknowledges the financial support by the Federal Ministry of Education and Research of Germany (BMBF) in the framework of YESPVNIGBEN project (03SF0576A).
D.L. was supported from European Regional Development Fund project "Plants as a tool for sustainable global development" (CZ.02.1.01/0.0/0.0/16_019/0000827).

Abstract

Foundations of photosynthesis research have been established mainly by studying the response of plants to changing light, typically to sudden exposure to a constant light intensity after a dark acclimation or to light flashes. This approach remains valid and powerful, but can be limited by requiring dark acclimation prior to time-domain measurements and often assumes that rate constants determining the photosynthetic response do not change between the dark- and light-acclimation.

We present experimental data and a mathematical model demonstrating that these limits can be overcome by measuring plant responses to sinusoidally modulated light of varying frequency. By its nature, such frequency domain characterization is performed in light-acclimated plants with no need for prior dark acclimation. Amplitudes, phase shifts and upper harmonic modulation extracted from the data for a wide range of frequencies can target different kinetic domains and regulatory feedbacks. The occurrence of upper harmonic modulation reflects non-linear phenomena, including photosynthetic regulation. To support these claims, we present a frequency and time domain response

[1] L.N. conceived the study, did the experiments, analyzed the experimental data, performed the analytical calculations, wrote parts of the manuscript and was responsible for finalizing it.
[2] D.L. performed the numerical calculations, analyzed the experimental data, wrote parts of the manuscript and supervised the literature screening and referencing.

in chlorophyll fluorescence emission of the green alga *Chlorella sorokiniana* in the frequency range 1000 – 0.001 Hz. Based on these experimental data and on numerical as well as analytical mathematical models, we propose that the frequency domain measurements can become a versatile new tool in plant sensing.

Introduction

The fundamental principles and structures performing oxygenic photosynthesis are highly conserved in all plants and algae. Diversity appears with adaptation and acclimation that are required for optimal performance in relevant climatic conditions, including dynamically changing light intensities and temperatures (Singsaas and Sharkey 1998, Cruz et al. 2016). Balancing linear and cyclic electron pathways among two serially operating photosystems in a dynamic environment requires elaborate regulation (Tikhonov 2015, Armbruster et al. 2017) to optimize yields and minimize potential damage by harmful by-products such as reactive oxygen species (Pospíšil 2016, Foyer 2018).

The dynamic complexity of photosynthesis is typically approached in the time-domain by studying responses that occur when dark-acclimated plants or algal cells are suddenly exposed to light. Chlorophyll (Chl) fluorescence induction that occurs upon light exposure is one of the most frequently used biophysical methods in plant physiology. The response to strong light, referred to in the literature as O-I_1-I_2-P (Neubauer and Schreiber 1987) or O-J-I-P transient (Strasser and Govindjee 1991), is very rapid, and consists of clearly discernable phases that can be analyzed using numerical deconvolution (Stirbet et al. 2018). Exposure to lower actinic light intensities common in the natural plant environment leads to a slower induction, called the Kautsky-Hirsch effect (Govindjee 1995), that can be combined with multi-turnover saturation pulses probing photochemical and non-photochemical quenching (reviewed in Lazár 2015). The spectrum of Chl fluorescence techniques is further enlarged by methods that apply single-turnover flashes (e.g., Kolber et al. 1998, Nedbal et al. 1999). Another important set of Chl fluorescence methods exploits time resolution even further using ultrashort flashes that allow resolution of primary photosynthetic processes in reaction centers (Chukhutsina et al. 2019).

The dynamic range that needs to be considered spans more than 19 orders of magnitude, from elemental energetic processes in the reaction centers (≈10^{-12} s), to regulation and acclimation processes that can be as slow as days (≈10^5 s) or seasons (≈10^7 s). Interpreting such a diversity of dynamic phenomena based on mathematical models is hindered by non-linear interactions that may link, e.g., slow regulation and fast primary processes. Another challenge in understanding photosynthesis dynamics is that thylakoids are far from rigid, with substantial conformational changes

in photosynthetic proteins occurring already within the first seconds of exposing dark-acclimated samples to light (Schansker et al. 2011, Suga et al. 2017, Magyar et al. 2018, Oja and Laisk 2020, Sipka et al. 2021). The system dynamics during this fast phase of induction is therefore determined not only by filling the charge pools or saturating the pathways but also by the systemic thylakoid re-arrangement, all leading to potential non-linearity of the investigated system. To describe this situation, one can discriminate between the constitutive non-linearity directly related to primary photosynthetic functions and regulatory non-linearity (Bich et al., 2016). The latter is due to regulatory interactions activated by a dedicated subsystem that is dynamically decoupled from the regulated one and that is not performing constitutive functions. With this categorization, energization of the thylakoid membrane, including cyclic electron transport and saturation of photosynthetic pathways, represents constitutive non-linearity because the involved processes constitute the primary function of photosynthetic apparatus. The non-photochemical quenching (NPQ) facilitated by dedicated PsbS and violaxanthin de-epoxidase systems responding to lumen acidification is a prime example of a regulatory process causing regulatory non-linearity (Demmig-Adams et al. 2014, Ruban 2016, van Amerongen and Chmelinov 2020). Sensing constitutive and regulatory dynamics in the time domain may require acclimation to darkness prior to illumination, a protocol that may limit many practically relevant applications in field or greenhouse. With few exceptions (van Kooten et al. 1986, Lebedeva et al. 2002, Lyu and Lazár 2017), interpreting the data by means of mathematical models requires assuming that the rate constants of photosynthetic processes do not change during induction, which contradicts mounting evidence for substantial conformational changes of photosynthetic proteins during the process (Schansker et al. 2011, Suga et al. 2017, Magyar et al. 2018, Oja and Laisk 2020, Sipka et al. 2021).

To avoid these drawbacks, one can consider studying the dynamic properties of photosynthesis in the frequency-domain by exposing plants and algae to sinusoidally[3] modulated light of a single angular frequency ω. This approach is a valid abstraction of fluctuating light environments appearing in nature due to sun flecks, movement of leaves by wind, shading of leaves by the canopy, or, with phytoplankton, waves on the water surface. From the perspective of mathematical modeling, harmonic modulation is convenient as it appears in Fourier transforms as a single sharp peak, making solution of model differential equations relatively easy (Schwartz 2008). Harmonic oscillations also appear in plant responses to sudden changes in the environment. Laisk and Walker suggested that "understanding oscillations means understanding photosynthesis" (Laisk and Walker 1989). Initially, focus was on spontaneous oscillations induced in plants by, e.g., an abrupt change in the gas phase

[3] We shall henceforth use the general term 'harmonically modulated' rather than the more restrictive term "sinusoidally modulated"

composition, and measured in Chl fluorescence, oxygen evolution, or CO_2 fixation (Walker et al. 1983, Walker and Sivak 1985, Sivak and Walker 1985, 1986, 1987, Malkin 1987). Several hypotheses have been suggested to explain the spontaneous oscillations (Lazár et al. 2005).

Studying forced oscillations is widely used in physics and engineering. A trivial example can be found in characterizing dielectrics, in which permittivity is measured by scanning over frequencies of a harmonically modulated electric field. This systemic homology is detailed in Supplementary Materials (SM3). The mathematical essentials connected to frequency-domain measurements and analysis are summarized in Supplementary Materials (SM2). Aiming to realize similar potential in photosynthesis research, we propose to complement or, whenever dark adaptation represents a problem, substitute time-domain studies of the dark-to-light transition with frequency-domain measurements of responses to harmonically modulated light.

Scanning over a range of frequencies can address individually dynamically contrasting processes. An additional strength of the proposed frequency-domain investigation is that the measured response can be selectively filtered by hardware or data processing to narrow the sensitivity range close to the forcing frequency of the excitation light (Litovski 2019). Hence, the frequency-domain measurements may provide a higher signal-to-noise ratio than time-domain measurements, which are, by their nature, spread over a broad band of frequencies that are inescapably present in dark-to-light transitions.

In this work, we present an experimental analysis of Chl fluorescence emission response in green alga *Chlorella sorokiniana* to harmonically modulated light in the range from 1000 to 0.001 Hz. The sub-range 1000 – 1 Hz is characterized for the first time. The observed constitutive non-linearity is investigated using a detailed mathematical model of primary photosynthetic reactions. Implications of the regulatory non-linearity are explored using a simplified, analytically solvable mathematical model of photosynthetic antenna regulation.

The capability of this approach to selectively sense processes within a specific range of rate constants, to sense regulation, and its high signal-to-noise ratio open new opportunities, particularly for broad daytime phenotyping, development of sentinel plants, and stress detection in field and greenhouse, all without a need for dark adaptation.

Results

Experiments

Contrasting types of Chl fluorescence yield response to harmonically modulated light measured in a suspension of *Chlorella sorokiniana* are illustrated in Figs. 1A-D. The algae were light-acclimated and the periodic response was largely stationary when measured. The graphs do not start at time 0 to indicate how long the acclimation to oscillating light before the sampling was. Figure 1A depicts the typical Chl fluorescence response to short period (1 s), low-amplitude light modulation (8 - 20%)[4]. Figure 1B depicts dynamics under high-amplitude (8 - 100%, 1 s) modulation. Figures 1C and 1D represent low-amplitude and high-amplitude modulations, respectively, for the longer period of 256 s. Each panel in Fig. 1 consists of two sub-panels with experimental data in the top and numerical analysis in the bottom. The top panels (A1, B1, C1, D1) depict the light modulation (red line) and the measured Chl fluorescence yield response (blue points). The least square fits of the measured data by a combination of up to four sinusoidal functions:

$$Fit(t) = A_0 + A_1 \cdot sin\left[\frac{2\pi(t-\tau_1)}{T}\right] + A_2 \cdot sin\left[\frac{4\pi(t-\tau_2)}{T}\right] + A_3 \cdot sin\left[\frac{6\pi(t-\tau_3)}{T}\right] + A_4 \cdot sin\left[\frac{8\pi(t-\tau_4)}{T}\right]$$

Eq. 1

are represented by thick gray lines in all bottom sub-panels of Fig. 1. The thin lines in panels A2, B2, C2, and D2 represent the individual harmonic components:

- the fundamental harmonics $A_0 + A_1 \cdot sin\left[\frac{2\pi(t-\tau_1)}{T}\right]$ by the thin black line;
- the first upper harmonics $A_0 + A_2 \cdot sin\left[\frac{4\pi(t-\tau_2)}{T}\right]$ by the thin red line;
- the second upper harmonics $A_0 + A_3 \cdot sin\left[\frac{6\pi(t-\tau_3)}{T}\right]$ by the thin green line
- the third upper harmonics $A_0 + A_4 \cdot sin\left[\frac{8\pi(t-\tau_4)}{T}\right]$ by the thin blue line.

[4] The light intensity scale is relative, defined in the instrument protocol in %. The minimum around 8% was found empirically to be the lowest protocol setting with a linear correspondence between protocol and light generated by the instrument. Relationship to the absolute number of PSII turnovers·s^{-1} and absolute light units is described in Materials and Methods.

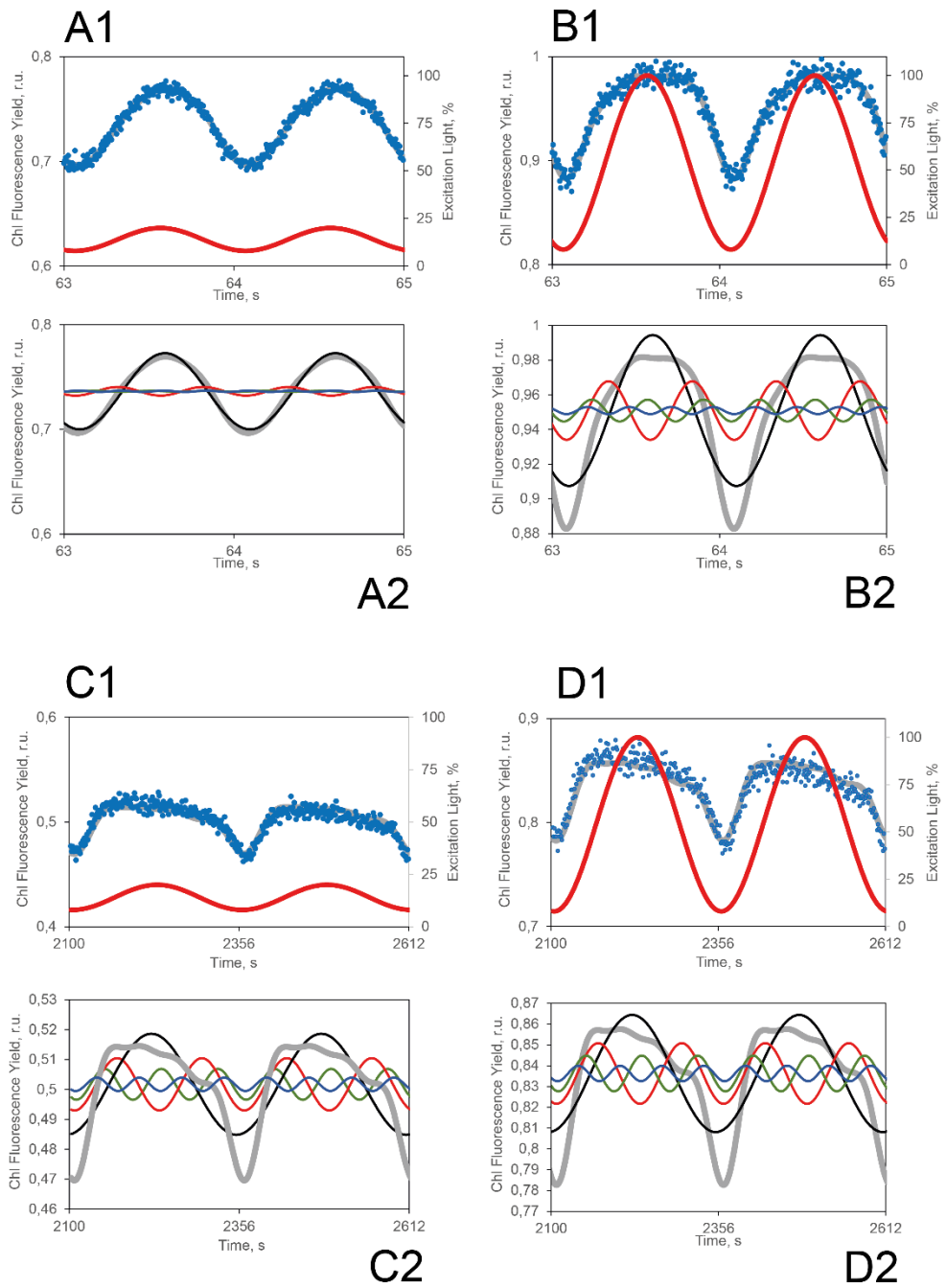

Figure 1. *The thick red lines in panels A1 and B1 show light modulation with a period of 1 second while panels C1 and D1 show a modulation period of 256 seconds. The amplitudes of light oscillations were low in panels A and C (min. 8%, max. 20%) and high (min. 8%, max. 100%) in panels B and D. The corresponding absolute values of photosynthetically active radiation are specified in Materials and Methods. The gray lines in both the top and bottom sub-panels represent numerical fitting of the experimental data by a superposition of one fundamental harmonic component ($\omega = \frac{2\pi}{T}$, thin black line) and up to 3 upper harmonic components: the thin red line with $\omega = 2 \cdot \frac{2\pi}{T}$, the thin green line with $\omega = 3 \cdot \frac{2\pi}{T}$, and the thin blue line with $\omega = 4 \cdot \frac{2\pi}{T}$. The essentials of the numeric analysis are described in detail in Supplementary Materials.*

The response to low-amplitude light oscillating with a period of 1 second (Fig. 1A1) is well fit by the fundamental harmonics, with negligible contributions from upper harmonic modes (Fig. 1A2).

Increasing the amplitude of the oscillating light leads to the appearance of an upper harmonic modulation (Fig. 1B1-2) that most likely has, at least to some extent, a trivial explanation by saturation of photosynthesis around the peak light. Interestingly, the upper harmonic modulation was found in the Ch fluorescence yield response to low-light (Fig. 1C) as well as to high light (Fig. 1D) when the period was 256 seconds. This finding is consistent with earlier reports of upper harmonic modulation occurring with long forcing periods in higher plants and cyanobacteria (Nedbal and Březina 2002, Nedbal et al. 2003, 2005).

Compared to earlier studies, we extend the range of investigated periods in Fig. 2 by at least three orders of magnitude and show the Chl fluorescence yield response for forcing periods between 1 millisecond and 1000 seconds using the same approach and data analysis as in Fig. 1.

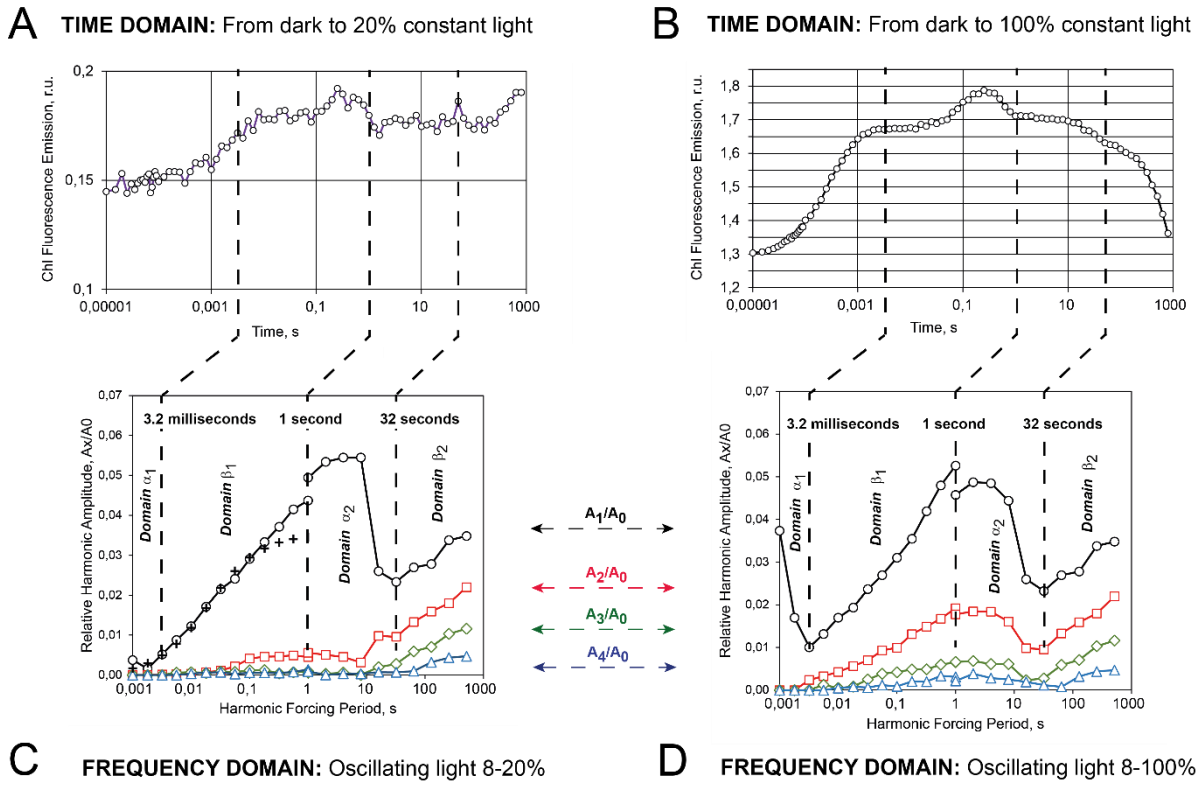

Figure 2. *Comparison of Chl fluorescence dynamics in* C. sorokiniana *measured in response to dark-to-light transition in the time domain (A, B) and in response to harmonically modulated light in the frequency domain (C, D). The color-coding of the fundamental and upper harmonic amplitudes is the same as in Fig. 1 and is also reflected in the legend between panels C and D.*

Figure 2 shows in panels A and B the Chl fluorescence transients measured after exposure of dark-adapted algae to constant light: 20% relative light intensity in panel A and 100% light intensity in panel B. Unlike all other Chl fluorescence measurements reported here, the Chl fluorescence emission shown in Fig. 2 A, B was excited directly by the actinic light and no measuring flashes were used. Identical measurements performed with 20%, 32%, 56% and 100% relative intensity and numerical analysis of

the initial photochemical phase of the transients (Lazár et al. 2001) revealed that the light was linearly increasing the photosystem II turnover rate between 20 and 100% in four equal steps and that 100% relative intensity induced 4930 photosystem II turnovers per second (R^2 = 0.9983). Additional details about effective photosynthetically active irradiance during the measurements are described in Materials and Methods.

The time-domain responses to the dark-to-light transition (Fig. 2A-B) are compared to the frequency responses to harmonically modulated light in panels C and D. The frequency response of photosynthesis by means of Chl fluorescence yield in Fig. 2 can be partitioned into four characteristic frequency domains: α_1 (periods ca. 1 ms - 3.2 ms), β_1 (periods ca. 3.2 ms – 1 s), α_2 (periods ca. 1 s – 32 s), and β_2 (periods ca. 32 s – 512 s). The harmonic components drop with increasing forcing period in domains α_1 and α_2 and increase in domains β_1 and β_2. The increase in the β_1 and β_2 domains is approximately linear in the logarithmic-linear graph in Fig. 2, indicating an exponential relationship in a linear-linear representation.

Heuristic use of the analogy to dielectric permittivity proposed in the Introduction and in Supplementary Materials (SM3-4) as well as considerations proposed in Nedbal and Březina (2002) indicate that the observed frequency dependence might be approximated by $\frac{\beta}{\sqrt{\beta^2+(\omega-\omega_0)^2}}$, where β and ω_0 are empirical parameters and $\omega = \frac{2\pi}{T}$ is the angular frequency of the light modulation. The numerical least-squares fitting in the β_1 domain by $\frac{\beta}{\sqrt{\beta^2+(\omega-\omega_0)^2}}$ is shown in Fig. 2C by black crosses. The quality of the fit is not perfect but the qualitative agreement with experimental data over two orders of magnitude suggests that the dispersion[5] in form common in the theory of dielectric permittivity can be indeed a good heuristic approach.

Another outstanding feature of the frequency response of photosynthesis is the appearance of upper harmonic modes (colored lines in Fig. 2C-D) that appear in two 'waves': the first increasing in the β_1 domain and decreasing in the α_2 domain, and the second monotonically increasing in the β_2 domain. We propose that the upper harmonic modes in β_1, α_2 and those in β_2 are of different molecular origin and use an earlier numerically-solvable model (Lazár 2009) to identify the mechanism of modulation in the β_1, α_2 domains and a new analytically solvable model to show that the upper harmonic modulation in the β_2 domain reflects biological regulation. Both models are graphically represented in Fig. 3.

[5] We adopt the term "dispersion" in the meaning common in the theory of dielectrics, i.e. as a dependence of an observable on the frequency or period of the forcing input, here of harmonically modulated light.

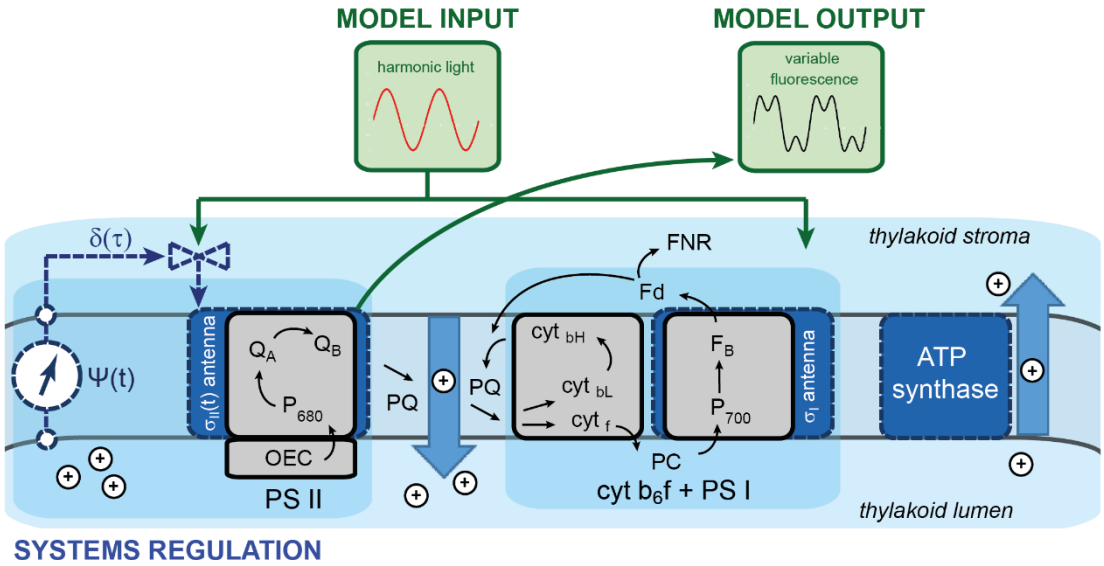

Figure 3. *Simplified graphical representation of the subsystems involved in photosynthesis in an algal thylakoid. The photosynthetic apparatus is exposed to harmonically modulated light (system input* $u(t) = u_0 + u_V \cdot \sin(\omega \cdot t)$*) that drives photochemical reactions in the two photosystems, which are responsible for linear and cyclic electron transport and, eventually, for generation of a difference of the electrochemical potential across the thylakoid membrane. The dynamic response of the system to harmonic forcing is measured by a fluorescence PAM-type sensor. The components considered in the numerically-solvable model (Lazár 2009) are shown in black letters. The blue shaded blocks represent the analytically-solvable model. Complex regulation of photosynthetic reactions is reduced in this scheme to a control of excitation of Photosystem II, which is called non-photochemical quenching (regulation* $\delta(t)$*). More details are explained in the respective parts of the text.*

Numerical solutions of a detailed molecular mathematical model

Detailed molecular models are available for numerical solutions of photosynthetic dynamics during the dark-light transition (Lazár and Schansker 2009, Stirbet et al. 2020) and here we modify the model of Lazár (2009) to additionally explore the dynamics in harmonically modulated light. This model describes electron transport in the thylakoid membrane through Photosystem II, cytochrome b_6/f and Photosystem I to ferredoxin and also cyclic transport (see the components and pathways indicated in Fig. 3 by black letters and arrows). This model was previously used for simultaneous simulation of fast Chl fluorescence induction (the O-J-I-P curve) and of the I_{820} signal that reflects redox state of primary electron donor in Photosystem I, P700, and of electron transporter plastocyanin (Lazár 2009).

The underlying set of differential equations in this model includes a number of non-linear terms that may lead to complex modulation in the Chl fluorescence response, i.e., the exchange of doubly reduced and protonated Q_B with plastoquinone molecules from the pool or electron transport from Photosystem I to ferredoxin. The model also captures saturation of photosynthetic reactions by high light intensities. These phenomena belong to the category of constitutive non-linearities (Bich et al. 2016).

Numerical simulations of forced oscillations of Chl fluorescence yield with a period of 100 ms are shown in Fig. 4, confirming the experimental observations in Fig. 1, namely that forcing by low-

amplitude light leads to a variation of Chl fluorescence yield that is very close to a simple sinusoidal function of the forcing period: Fig. 1A for experiment and Fig. 4A for the numerical model. Remaining to be explained by future improved models is the large phase shift between the light and Chl fluorescence response predicted in Fig.4A and not confirmed by the experiment (Fig.1A1).

Substantial deviations from sinusoidal dynamics were observed under strong high-amplitude light modulation (see Fig. 1B (experiment) and Fig. 4B (model)). This deviation was clearly visible in the appearance of upper harmonic modes in the experimentally observed dynamics as well as in the model prediction.

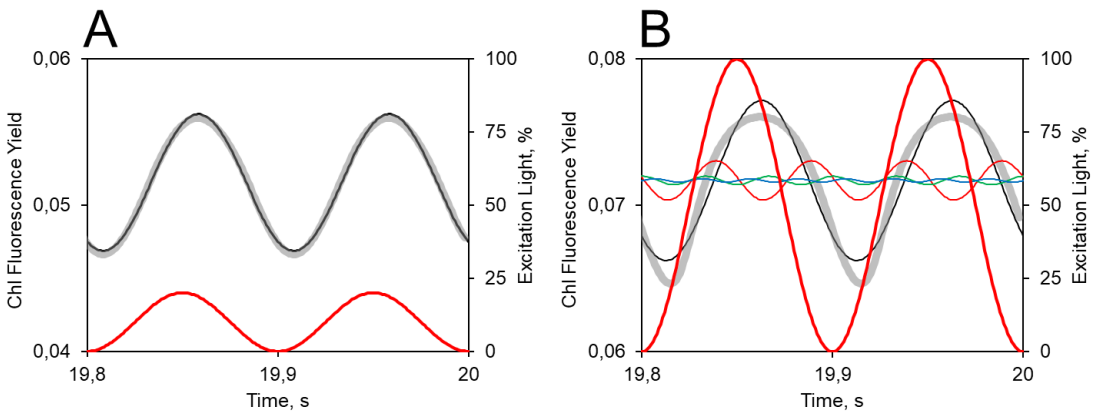

Figure 4. *Modeled Chl fluorescence yield response (thick gray lines) to harmonically modulated light (thick red lines) of low (A) and high amplitude (B). The thin black and colored lines show the result of a least-squares fitting of the modeled dynamics. Color code and fitting functions are the same as in Fig. 1.*

Interestingly, the model predicts that Chl fluorescence modulation amplitude increases with periods increasing from near zero at 1 ms to nearly maximum at 100 s (Fig. 5, black solid line). A rise was also observed experimentally in the β1 domain (3.2 ms - 1 s) (Fig. 2C and green line in Fig.5). However, the model-predicted curve is significantly steeper than the one observed experimentally (Fig. 5, cf. black and green solid lines). Figure 5 also allows comparison of the phase shifts between oscillating light components and Chl fluorescence response predicted by the model (Fig. 5, black dashed line) and observed experimentally (Fig. 5, green dashed line). The model prediction (black dashed line) qualitatively agrees with experiment in trend and amplitude but fails quantitatively and also suggests an inflection in the dispersion that is not seen in the experiment.

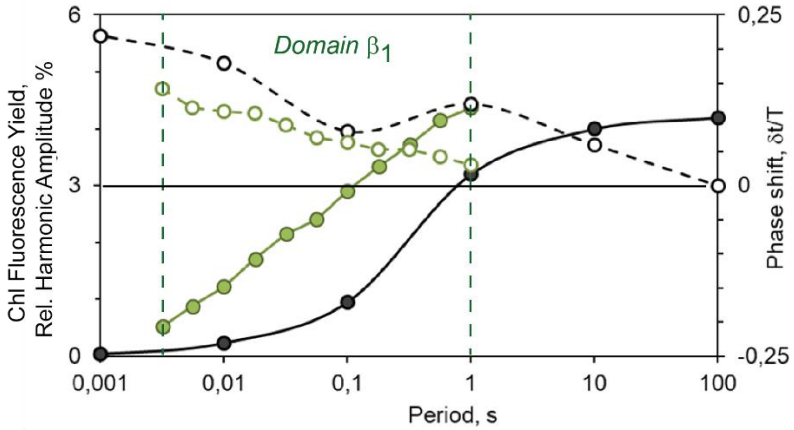

Figure 5. *Comparison of the model-predicted dispersion (see footnote 4 for term explanation) in the amplitude (solid line) and phase (dashed line) of the Chl fluorescence yield response of photosynthetic apparatus to forcing by harmonically modulated light (black lines) with experimental observation (green lines).*

The numerical model is also a potent tool for exploring the dynamics of components not directly observed in the present experiments. A simulated comparison between the closely related Chl fluorescence yield dynamics and plastoquinone redox state is modeled in Fig. 6. Two low-amplitude harmonic light forcing periods were selected for the simulation. The model predicts that light modulation with a period of 0.1 s leads to a simple sinusoidal modulation of Chl fluorescence yield (Fig. 6A), a prediction which agrees with the already presented experimental (Fig. 2) as well as modeling results (Fig. 4). Modulation of the plastoquinone-pool is predicted by the model to be of a very small amplitude (green line in Fig. 6A). This strong damping of plastoquinone redox dynamics is dictated by the size of the plastoquinone pool relative to variations in the in- and outflux of electrons. The large stability of plastoquinone redox state suggested by the green line in Fig. 6A can also indicate that the in- and outflux of electrons in the plastoquinone pool in the short period are largely balanced and synchronized so that the changing light has little effect on the plastoquinone pool redox state. With an increase in the light period to 1 s (Fig. 6B), the fraction of reduced plastoquinone molecules in the pool starts to oscillate strongly and drops sharply around the light minima (green light in Fig. 6B).

The differences between Chl fluorescence dynamics and plastoquinone reduction dynamics (cf. blue and green lines in Fig. 6) underscore the conclusion that measuring the Chl fluorescence signal alone may not be enough to fully elucidate molecular mechanisms that are decisive in a fluctuating light environment. Measurement of additional reporter signals as well as improved mathematical modeling will be necessary to fully understand the dynamics in oscillating light.

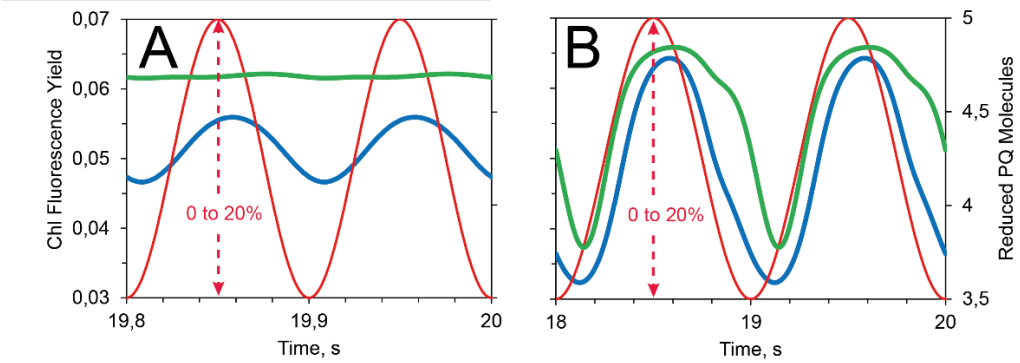

Figure 6. *Dynamics of Chl fluorescence yield (blue) and of reduced plastoquinone molecules (green) predicted for light forcing periods of 0.1 s (A) and 1 s (B), and Photosystem II turnover time corresponding to 20% light in Figs .2A,C. These predictions were generated using the model described in (Lazár 2009). Interesting dynamic details of the plastoquinone reduction in 0.1s modulation (green line in A) are shown in Supplementary Materials (SM1) on an expanded scale.*

Analytical mathematical model

Complex non-linear mathematical models such as the one discussed in the previous paragraphs can only be solved numerically, and a large number of simulations, control analysis, and other advanced mathematical tools are needed for predicting which components contribute to any particular dynamic behavior and by how much. These models are moreover often based on limited knowledge about the true values of the rate constants and most of them assume that the rate constants do not change while the photosynthetic apparatus undergoes induction. These are the deficiencies may explain why agreement between experiment and the detailed model predictions is limited (Fig. 5). This situation by no means delegitimizes the detailed molecular models, rather it suggests that both the detailed bottom-up modeling approaches as well as the top-down approach presented in this section are needed to reflect the different hierarchical levels of the modeled system.

Considering this situation and inspired by the small number and the apparent simplicity of the dynamic features found in the frequency response of photosynthesis (Figs. 1 and 2), we constructed a highly simplified mathematical model of the photosynthetic light reactions that may nevertheless qualitatively simulate this behavior. The essential components of the model are shown in Fig. 3 in blue symbols and letters and, in more detail in Supplementary Materials (SM4).

In a zero-level model approximation, the NPQ regulation of the antenna is assumed to be negligible ($\delta \approx 0$) and the relationship between the electrochemical potential difference across the thylakoid membrane $\Psi_0(t)$ and light $u_0 + u_V \cdot sin(\omega \cdot t)$ (see Fig. SM2) appears as a linear ordinary differential equation:

$$\left(u_0 + u_V \cdot sin(\omega \cdot t)\right) - \alpha \cdot \left(\frac{d\Psi_0(t)}{dt} + \beta \cdot \Psi_0(t)\right) = 0 \qquad \text{Eq. 2}$$

The parameters α and β are shown in the Supplementary Materials (SM4) to depend on the effective size of the photosynthetic antennae, the stoichiometry of coupling between electron and proton

transport, the capacitance of the thylakoid membrane and the rate of ATP-synthesis. Solution of Eq. 2 is derived in detail in Supplementary Materials (SM4). In a stationary limit ($t \gg 1/\beta$) that corresponds to the experiments shown in Fig. 1 and 2, the solution can be expressed as:

$$\Psi_0(t) = \frac{u_0}{\alpha \cdot \beta} + \frac{u_V}{\alpha} \cdot \left[\frac{1}{\sqrt{\beta^2+\omega^2}} \cdot sin\left(\omega \cdot t - arccos\frac{\beta}{\sqrt{\beta^2+\omega^2}}\right)\right] \quad \text{Eq. 3}$$

The model thus predicts that with low-amplitude light modulation and without regulation, $\Psi_0(t)$ will be modulated as a simple sinusoidal function shifted by $arccos\frac{\beta}{\sqrt{\beta^2+\omega^2}}$ in time relative to the light modulation sinus (Eq. 3). No upper harmonic modulation is predicted by the model in the absence of photosynthetic regulation. This prediction qualitatively agrees with the experimental observations in low-light amplitudes and short periods in the domain β_1 shown in Fig. 1A and Fig. 2.

Regulation of Photosystem II antenna size $\delta(\tau)$ approximating NPQ and assumed to be controlled by the electrochemical potential across the thylakoid membrane (Fig. 3), is an example of an interaction that leads to a non-linearity between system output (here Chl fluorescence emission or the electrochemical potential) and light input. This non-linearity originating from regulation contrasts with the previously discussed trivial constitutive non-linearity that occurs due to saturation of the photosynthetic pathways in strong light or due to non-linear primary photosynthetic reactions (Fig. 1B).

With regulation ($\delta > 0$), the equation becomes more complex:

$$u_V \cdot sin(\omega \cdot t) - \alpha \cdot \left(\frac{d\Phi(t)}{dt} + \beta \cdot \Phi(t)\right) = \Delta \cdot \Phi(t) \cdot \left[u_0 \cdot \left(1 - \frac{1}{\alpha\beta}\right) + u_V \cdot sin(\omega \cdot t) - \Phi(t)\right] \quad \text{Eq. 4}$$

, where $\Phi(t)$ is the variable part of the electrochemical potential $\Psi(t)$ and $\Delta = s/2\sigma$ a constant that can, in a specific model, replace the time-variable regulation function *δ(t)* that was introduced in Fig. 3 (for details, see Supplementary Materials, SM4, Eq. SM25a-c). Equation 4 is a first-order ordinary differential equation that is quadratic in the function $\Phi(t)$ and as such belongs to the Riccatti-type of differential equation (Reid 1972). It would be possible to continue with further approximations and iterations towards a more accurate analytical solution but such an effort exceeds the scope and ambition of the present publication. Remarkably, the photosynthetic response to harmonically modulated light can be always deconvolved into a small number of upper harmonic modes, making the dynamics "bumpy", i.e. with clearly discernable shoulders or even local maxima (see also Nedbal and Březina, (2002) for experimental results with higher plants and cyanobacteria). Additionally, the numerical analysis presented in Supplementary Materials (SM2) confirms that the periodic transients can be expected to consist of a small number of upper harmonic modes. Assuming that the regulation is weak ($1 \gg \Delta > 0$), this feature suggests that a solution of Eq. 4 can be sought iteratively in form of a small number of Taylor series terms: $\Psi(t) \approx \Psi_0(t) + \Delta \cdot \Psi_1(t) + \Delta^2 \cdot \Psi_2(t) + \cdots$

As shown in Supplementary Materials (SM4), this approximation can be used to show that the first term in the Taylor series leads to an appearance of the first upper harmonic mode (in bold):

$$\Delta \cdot \Psi_1(t) = \Delta \cdot [A(\omega, \alpha, \beta, u_0, u_v) \cdot sin(\omega \cdot (t - \tau_A(\omega, \alpha, \beta, u_0, u_v)) + \boldsymbol{B(\omega, \alpha, \beta, u_0, u_v)} \cdot \boldsymbol{sin(2 \cdot \omega \cdot (t - \tau_B(\omega, \alpha, \beta, u_0, u_v))}] \quad \text{Eq. 5}$$

The term in Eq. 5 containing the first upper harmonic mode (2ω) proportional to Δ that represents the regulation depicted in Fig. 3. Mathematically, the identical procedure can be used to show that the second and third upper harmonic terms ($3\omega, 4\omega$) appear proportional to Δ^2 and Δ^3. This means that, with a weak regulatory interaction ($1 \gg \Delta > 0$) the upper harmonic modes appear with amplitudes rapidly decreasing with increasing order. The model-supported small number of relevant upper harmonic modes may thus explain the "bumpy" character of the observed photosynthetic response (Nedbal and Březina, (2002) and Figs. 1 and 2).

Equation 4 was derived using multiple crude approximations and additionally the variable part of the electrochemical potential $\Phi(t)$ affects the Chl fluorescence emission only indirectly, by NPQ modulation. The main conclusion is however general: Regulation will introduce in the model differential equations products of light modulation (system input) with system variables ($\Phi(t)$ here or Q_A or PQ pool redox states elsewhere) and squares of systems variables as in Eq. 4. These terms will lead, in the case of harmonic modulation of light, to an appearance of upper harmonic modes in system observables.

Discussion

Forced Chl florescence oscillations, i.e. the Chl fluorescence response to harmonically modulated light, has been so far studied only rarely, with studies in higher plants and cyanobacteria resolving detailed dynamics limited to periods longer than 1 s (Nedbal and Březina 2002, Nedbal et al. 2003, 2005, Shimakawa and Miyake 2018, Samson et al. 2019). This study extends the dynamic range to cover nearly 6 orders of magnitude: 1000-0.001 Hz in frequency and 0.001 – 1000 s in periods, and was performed with a green alga.

Interestingly, green algae in high-frequency, square modulated light were investigated also earlier by Nedbal et al. (1996) searching for enhancement of photosynthetic rates predicted by the enigmatic flashing light effect (Kok 1953). The conclusion of this early work was that with frequencies approaching 1000 Hz, photosynthesis approached levels that would occur in continuous equivalent light. This was tentatively interpreted as showing that light modulation in this frequency range is integrated by the photosynthetic apparatus. The experiments as well as mathematical model results presented in the present study confirm this earlier hypothesis both experimentally and computationally.

The experimental evidence (Figs. 1 and 2) for the dynamic behavior in the domains β_1 (periods 3.2 ms – 1 s), α_2 (periods 1 – 32 s), and β_2 (periods 32 s – 512 s) is strong. However, the discrepancy between model and experiment found in the α_1 domain for periods 1 ms – 3.2 ms (Fig. 2) needs to be re-examined with alternate instrumentation as it was measured at an extreme limit of the present instrument range. With this exception, the data in Fig. 2 are robust and were obtained with different exponentially and late-exponentially growing cultures with little quantitative variability, represented here by the small discontinuity at a period of 1 s. Additionally, the scanning direction was alternating, from short to long periods as well as in the opposite direction. Negative controls were measured with algae that were inactivated by heating to 60 – 80 °C for 10 minutes and, without exception, confirmed absence of any variable Chl fluorescence, confirming that Photosystem II was inactive. Each measuring protocol was also applied to the heat-inactivated samples and the fluorescence yield was confirmed to be independent of any light modulation. In addition to the scanning protocols used to generate the data presented above, measurements were individually performed for each period and amplitude, always with a fresh sample aliquot. Each measurement was repeated three times leading to Bode[6] plots as in Fig. 2. Importantly, two additional intermediate light amplitude modulations were investigated, namely from 8-32% and 8-54% in addition to the 8-20% and 8-100% modulations shown in Figs. 2C and D, respectively. These two additional intermediate light levels were already strong enough to nearly saturate the photosynthetic pools but did not exhibit the photoinhibitory decline in Chl fluorescence during the long exposure 32 – 1000 s (Fig. 2B). In all other aspects these additional experiments independently confirmed the dynamic behavior in saturating light shown in Fig. 2D.

The Bode plots in Fig. 2C and Fig. 5 observed experimentally contrast with the much steeper slopes suggested by the mathematical model (cf. solid green and black lines in Fig. 5). This important qualitative mismatch indicates that models developed for dark-to-light transitions must be amended to correctly describe the dynamic behavior in light-acclimated photosynthetic organisms.

Comparison of time-domain (Fig. 2A, B) with frequency-domain measurements (Fig. 2C,D) reveals that the latter can provide information on upper harmonic modes that is unavailable in the conventional PAM time-domain. The information content of the time-domain data can be increased, e.g., by use of saturating pulses, but the same is also possible in the frequency-domain where other dynamic reporters such as the I_{820} signal, CO_2 assimilation rate, non-photochemical quenching and other readouts can be measured (Nedbal et al. 2003).

The proposed frequency-domain approach to photosynthetic dynamics and regulation is not only technically advantageous but may contribute to understanding the important phenomena occurring

[6] The Bode plot is a graphical representation of frequency dependence of observables that is widely used in control theory.

in natural fluctuating day light (Vialet-Cahbrand et al. 2017, Annunziata et al. 2018, Wang et al. 2020) or artificial edge changes in irradiance (Cruz e al. 2016, Adachi et al. 2018, Li et al. 2020). Irradiance fluctuations affect photosynthetic performance and can reveal phenotypes that are not detectable under constant irradiance. Understanding the dynamics of regulation under fluctuating irradiance is essential to improve photosynthetic performance in natural conditions (Rascher and Nedbal 2006, Kaiser et al. 2018, Matsubara 2018, Slattery et al. 2018).

Conclusions

Frequency-domain measurements have a high potential for characterizing light-acclimated plants and algae, do not require prior dark adaptation, and are of intrinsically high signal-to-noise ratio. We propose that, as already established in engineering and physics, emancipating the frequency-domain approach in photosynthesis research can release significant potential.

Materials and Methods

Experimental measurements

Chlorella sorokiniana SAG 211-8k was obtained from Göttingen University culture collection and the precultures were inoculated from a Tris-Acetate-Phosphate nutrient medium (TAP) agarose plate and cultivated in TAP medium for 20 h at 30 ˚C in Erlenmeyer flasks (Andersen 2005). The experimental cultures were grown in the same medium but without acetate in a laboratory-build 700 mL column photobioreactor sparged by air. The culture temperature was stabilized at 22°C and irradiance of 200 μmol(photons)$\cdot m^{-2}\cdot s^{-1}$ was provided by an array of cold white light emitting diodes. The growth was monitored by measuring optical density in a 1 cm cuvette at 750 nm and the culture was daily diluted for sustained exponential grows. Aliquots of the suspension were sampled and diluted approximately to the optical density 0.3 to 0.5 before the measurements. The measurements of Chl fluorescence emission was performed as described in detail in (Nedbal et al. 2005) using a version of the double-modulation fluorometer (Trtílek et al. 1997) that was custom-modified to generate diverse actinic light patterns. The actinic light of 620 nm was either constant (only in Fig. 2A-B) or harmonically modulated with periods between 1 ms to 512 s (all other experiments). The fidelity of sinusoidal modulation was estimated by numerical fitting of the Chl fluorescence emitted by heat-inactivated algae (10 min. 60 – 80 °C) that was measured without measuring flashes. The deviations from sinusoidal functions were smaller than 2% when the minimum light intensity during the modulation was 8% and above. The scale of light intensity in the measurement cuvette of the instrument was quantified by calculating the numbers of turnovers elicited in Photosystem II per second with 20%, 32%, 56%, and 100% relative intensity. The numerical analysis of the initial photochemical phase of the transients (Lazár et al. 2001) revealed that the light was linearly increasing the Photosystem II turnover rate between 20 and 100% in

four equidistant steps and that 100% relative intensity induced 4930 Photosystem II turnovers in a second (R^2 = 0.9983). This number of turnovers is typically reached in higher plants by ca. 5000 μmol(photons)·m^{-2}·s^{-1} (Lazár 2003). With this and considering that the instrument zero, i.e., dark was at about 8% intensity setting, one can estimate effective levels of the oscillating light to be:

8 – 20% corresponding to oscillations effectively between 0 and 652 μmol(photons)·m^{-2}.s^{-1};

8 – 32% to oscillations effectively between 0 and 1304 μmol(photons)·m^{-2}.s^{-1};

8 – 56% to oscillations effectively between 0 and 2608 μmol(photons)·m^{-2}.s^{-1};

8 – 100% to oscillations effectively between 0 and 5000 μmol(photons)·m^{-2}.s^{-1};

The Chl fluorescence dynamics was quantified by relative quantum yield that was measured as Chl fluorescence increment generated by 4.5 μs-long measuring flashes that were added to the harmonically modulated actinic light at defined positions of the period. The stability of the measuring flashes on the background of harmonically modulated actinic light was another instrument feature that was checked to avoid artifacts. We assessed this stability by measuring, for each protocol setting and for each period of modulation, Chl fluorescence elicited by the flash in heat-inactivated algae that exhibited no change in yield over the measuring period. The stability was better than 1%.

The experimental protocols were using 200 measuring flashes per actinic light period, only with the shortest periods 1-10 ms, the number of flashes per period was reduced to 100.

Two types of protocols were used to demonstrate that the measurement results were independent of the protocol. The first type was designed to probe response with a particular period of harmonic light forcing T. It started with induction achieved by 60 periods T_{ind}=1s of actinic light. The Chl fluorescence response to a particular selected angular frequency $\omega = \frac{2\pi}{T}$ was then probed by applying 5 or 10 periods T. Only the last three periods were considered approximately stationary and used for further numerical analysis that was done by least-square fitting by Solver in Microsoft Excel.

The second protocol type was designed for scanning over many light modulation periods and was used in two variants: The first protocol variant was starting with induction by 100 periods of T_{ind}=1s of actinic light that were followed by ten measuring periods, each of T = 1000, 562, 316, 178, 100, 56, 32, 18, 10, 5.6, 3.2, 1.8 and 1 ms. The second protocol variant was also starting with induction by 100 periods of T_{ind}=1s of actinic light, followed by five measuring periods for T = 1, 2, 4, 8, 16, 32, 64, 128, 256, and 512 s.

Numerically Solved Model

The numerically solved model used in this work is the model originally published in Lazár (2009). Original goal for construction of the model was to show, by means of mathematical simulations, that electron transport in and beyond photosystem II shapes decisively the O-J-I-P Chl fluorescence

transient. The argument required parallel measurement of I_{820} transmission signal. Transmission at 820 nm is modulated by the redox state of primary electron donor in photosystem I (P700), and plastocyanin.

To describe this, the model had to consider the electron transport including: photosystem II with oxygen evolving complex, cytochrome b_6/f and photosystem I protein complexes, plastoquinone pool in the thylakoid membrane, plastocyanin in lumen and ferredoxin and ferredoxin-NADPH-oxidoreductase in stroma (see Fig. 3). Function of particular complexes is described by redox reactions between the four S-states (S_0, S_1, S_2, S_3) for oxygen evolving complex, between the primary electron donor, P680, and the first and the second quinone electron acceptors, Q_A and Q_B, respectively, for Photosystem II, between heme f, low and high potential hemes b, and heme c for cytochrome b_6/f, and between primary electron donor, P700, and iron-sulfur center F_B, for photosystem I. Since the electron donors and acceptors are fixed in the proteins, electron transport between them is described by the first order kinetics where each redox state of a protein represents combination of redox states of its electron carriers. For example, the initial redox state of photosystem II is described as $P680Q_AQ_B$, which is transformed to $P680^+Q_A^-Q_B$ due to the charge separation caused by absorption of light. Thus, photosystem II has 2 (P680, $P680^+$) x 2 (Q_A, Q_A^-) x 3 (Q_B, Q_B^-, Q_B^{2-}) = 12 states, time evolution of each of them being described by a differential equation. Similarly, cytochrome b_6/f has 12 states, and photosystem I 4 states. Electron transport to/from plastoquinone pool, plastocyanin and ferredoxin is described by the second order kinetics. Not to complicate photosystem II description by additional multiplication number of its states by 4 (for 4 S-states of oxygen evolving complex), electron transport during the S-states transition to $P680^+$ is described by the second order kinetics. Ferredoxin-NAPDH oxidoreductase is initially oxidized and inactive and after its activation it is consequently reduced twice by electrons from ferredoxin and the turnover of doubly reduced Ferredoxin-NAPDH oxidoreductase to active oxidized Ferredoxin-NAPDH oxidoreductase (the first order kinetics) reflects NADPH formation. To be able to simulate the Chl fluorescence data in agreement with the experiments, cyclic electron transport from ferredoxin directly to plastoquinone pool was considered (see Fig. 3), described by third order kinetics (electrons from two reduced ferredoxin molecules are necessary to reduce one plastoquinone molecule). Altogether, the model is a set of 42 ordinary differential equations, which was solved numerically in Matlab (MathWorks, USA). The oscillating excitation light enters the model in time-dependent value of rate constants of charge separation in photosystem II and photosystem I, i.e., in reaction $P680Q_AQ_B^{(-,2-)} \rightarrow P680^+Q_A^-Q_B^{(-,2-)}$ for photosystem II and in reaction $P700F_B \rightarrow P700^+F_B^-$ for photosystem I. The rate constants equal to $k_{max} \times 0.5 \times (1 - \cos(2 \times \pi \times t/T))$, where k_{max} is maximal value of the rate constant (equal to 100 or 500 s^{-1} for simulations in Figs. 4A and 6 and in Fig. 4B, respectively), which is proportional to intensity of excitation light (100% intensity ≈ k_{max} = 500 s^{-1}), and T is period of the oscillations (equal to 0.1 s for simulations in Figs. 4A, 4B, and 6A,

and 1 s in Fig, 6B, respectively), and t is time. Values of the other rate constants and initial conditions were taken from the literature (see Lazár 2009). Quantum yield of Chl fluorescence, which is shown in Figs. 4 and 6 and to which the experimentally measured Chl fluorescence signal was proportional, was defined as $\Phi_F(t) = \Phi_0 \times \Sigma Q_A(t) + \Phi_M \times \Sigma Q_A^-(t)$, where Φ_0 (= 0.02) and Φ_M (= 0.08, Lazár 1999) are quantum yields of Chl fluorescence when Photosystem II reaction centers are open (i.e., with Q_A) or closed (i.e., with Q_A^-), respectively and $\Sigma Q_A(t)$ and $\Sigma Q_A^-(t)$ are sums of all photosystem II states with Q_A and Q_A^-, respectively.

Acknowledgements

In addition to the acknowledgements to funding agencies stated elsewhere, the authors appreciate critical reading and feedback of Silvia Schrey, Shizue Matsubara, and Steven (Dean) Calahan from Forschungszentrum Jülich in Germany, Jakub Nedbal from King's College London in UK, and Johan Grobbelaar from University of Orange Free State, S.Africa. Validation of our mathematical derivations was done by Antonín Slavík from Faculty of Mathematics and Physics, Charles University Prague, Czech Republic. Language was thoroughly edited by Steven (Dean) Calahan.

References

Adachi S., Tanaka Y., Miyagi A., Kashima M., Tezuka A., Toya Y., Kobayashi S., Ohkubo S., Shimizu H., Kawai-Yamada M., Sage R.F., Nagano A.J., Yamori W. (2019) High-yielding rice Takanari has superior photosynthetic response to a commercial rice Koshihikari under fluctuating light. Journal of Experimental Botany 70, 5287-5297

Andersen R.A. ed. (2005) Algal culturing technique. Academic Press, Elsevier

Annunziata M.G., Apelt F., Carillo P., Krause U., Feil R., Koehl K., Lunn J.E., Stitt M. (2018) Response of Arabidopsis primary metabolism and circadian clock to low night temperature in a natural light environment. Journal of Experimental Botany 69, 4881-4895

Armbruster U., Galvis V.C., Kunz H.-H., Strand D.D. (2017) The regulation of the chloroplast proton motive force plays a key role for photosynthesis in fluctuating light. Current Opinion in Plant Biology 37, 56-62

Baba W. Kompala-Baba A., Zabochnicka-Swiatek M., Luzniak J., Hanczaruk R., Adamski A., Kalaji H.M. (2019) Discoveries trends in photosynthesis using modern analytical tools: More than 100 reasons to use chlorophyll fluorescence. Photosynthetica 57, 668-679

Bich L., Mossio M., Ruiz-Mirazo K., Moreno A. (2016) Biological regulation: controlling the system from within. Biology and Philosophy 31**,** 237-265

Chukhutsina V.U., Holzwarth A.R., Croce R. (2019) Time-resolved fluorescence measurements on leaves: principles and recent developments. Photosynthesis Research 140, 355-369

Cruz J.A., Savage L.J., Zegarac R., Hall C.C., Satoh-Cruz M., Davis G.A., Kovac W.K., Chen J., Kramer D.M. (2016) Dynamic environmental photosynthetic imaging reveals emergent phenotypes. Cell Systems 2, 365-377

Demmig-Adams B., Garab G., Adams III W.W., Govindjee, eds. (2014) Non-photochemical quenching and energy dissipation in plants, algae and cyanobacteria. Springer

Foyer C.H. (2018) Reactive oxygen species, oxidative signaling and the regulation of photosynthesis. Environmental ne Experimental Botany 154, 134-142

Govindjee (1995) Sixty-three years since Kautsky: chlorophyll *a* fluorescence. Australian Journal of Plant Physiology 22, 131-160

James F.A.J.L., ed. (1996) The Correspondence of Micheal Faraday, Volume 3, 1841-1848, Letter 1674, pp. 317-318. The Institution of Electrical Engineering and Technology, London, United Kingdom

Kaiser E., Morales A., Harbinson J. (2018) Fluctuating light takes crop photosynthesis on a rollercoaster ride. Plant Physiology 176, 977-989

Kok B. (1953) Experiments on photosynthesis by *Chlorella* in flashing light. In: Algal Culture from Laboratory to Pilot Plant, Burlew J.S. (ed.), 63-75. Carnegie Institution of Washington, Washington DC

Kolber Z.S., Prášil O., Falkowski P.G. (1998). Measurements of variable chlorophyll fluorescence using fast repetition rate techniques: defining methodology and experimental protocols. Biochimica et Biophysica Acta -Bioenergetics, 1367, 88-106

Laisk A., Walker D.A. (1989): A mathematical model of electron transport. Thermodynamic necessity for photosystem II regulation: 'light stomata'. Proceeding of the Royal Society B 237, 417-444

Lazár D. (1999) Chlorophyll *a* fluorescence induction. Biochimica et Biophysica Acta 1412, 1-28

Lazár D. (2003) Chlorophyll *a* fluorescence rise induced by high light illumination of dark-adapted plant tissue studied by means of a model of photosystem II and considering photosystem II heterogeneity. Journal of Theoretical Biology 220, 469-503

Lazár D. (2006) The polyphasic chlorophyll *a* fluorescence rise measured under high intensity of exciting light. Functional Plant Biology 33, 9-30

Lazár D. (2009) Modelling of light-induced chlorophyll *a* fluorescence rise (O-J-I-P transient) and changes in 820 nm-transmittance signal of photosynthesis. Photosynthetica 47, 483-498

Lazár D. (2015) Parameters of photosynthetic energy partitioning. Journal of Plant Physiology 175, 131-147

Lazár D., Kaňa R., Klinkovský T., Nauš J. (2005) Experimental and theoretical study on high temperature induced changes in chlorophyll *a* fluorescence oscillations in barley leaves upon 2 % CO_2. Phtosynthetica 43, 13-27

Lazár D., Schansker G. (2009) Models of chlorophyll *a* fluorescence transients. In: Laisk A., Nedbal L., Govindjee (eds.) Photosynthesis *in silico*: understanding complexity from molecules to ecosystems, pp. 85-123, Springer, Dordrecht

Lazár D., Tomek P., Ilík P., Nauš J. (2001) Determination of the antenna heterogeneity of Photosystem II by direct simultaneous fitting of several fluorescence rise curves measured with DCMU at different light intensities. Photosynthesis Research 68**,** 247–257

Lebedeva G.V., Belyaeva N.E., Demin O.V., Riznichenko G.Y., Rubin A.B. (2002) A kinetic model of primary photosynthetic processes. Description of the fast phase of chlorophyll fluorescence induction under different light intensities. Biophysics 47, 1044-1058

Li J., Tietz S., Cruz J.A., Strand D.D., Xu Y., Chen J., Kramer D.M., Hu J. (2019) Photometric screens identified Arabidopsis peroxisome proteins that impact photosynthesis under dynamic light conditions. Plant Journal 97, 460-474

Litkovski V. (2019) Electronic filters. Springer Singapore.

Lyu H., Lazár D. (2017) Modeling the light-induced electric potential difference (ΔΨ), pH difference (ΔpH) and proton motive force across the thylakoid membrane in C3 leaves. Journal of Theoretical Biology 413, 11-23

Magyar M., Sipka G., Kovács L., Ughy B., Zhu Q., Han G., Špunda V, Lambrev P.H., Shen J.-R., Garab G. (2018) Rate-limiting steps in the dark-to-light transition of Photosystem II - revealed by chlorophyll-*a* fluorescence induction. Scientific Reports 8, 2755

Malkin S. (1987) Fast photoacoustic transients from dark-adapted intact leaves: oxygen evolution and uptake pulses during photosynthetic induction – a phenomenology record. Planta 171, 65-72

Matsubara S. (2018) Growing plants in fluctuating environments: why bother? Journal of Experimental Botany 69, 4651-4654

Nedbal L., Březina V. (2002) Complex metabolic oscillations in plants forced by harmonic irradiance. Biophysical Journal 83, 2180-2189

Nedbal L., Březina V., Adamec F., Štys D., Oja V, Laisk A., Govindjee (2003) Negative feedback regulation is responsible for the non-linear modulation of photosynthetic activity in plants and cyanobacteria exposed to a dynamic light environment. Biochimica et Biophysica Acta -Bioenergetics 1607, 5-17

Nedbal L., Březina V., Červený J., Trtílek M. (2005) Photosynthesis in dynamic light: systems biology of unconventional chlorophyll fluorescence transients in *Synechocystis* sp. PCC 6803. Photosynthesis Research 84, 99-106

Nedbal L., Tichý V., Xiong F., Grobbelaar J.U. (1996) Microscopic green algae and cyanobacteria in high-frequency intermittent light. Journal of Applied Phycology 8, 325-333

Nedbal L., Trtílek M., Kaftan D. (1999) Flash fluorescence induction: a novel method to study regulation of photosystem II. Journal of Photochemistry and Photobiology B: Biology 48, 154-157

Neubauer C., Schreiber U. (1987) The polyphasic rice of chlorophyll fluorescence upon onset of strong continuous illumination: I. Saturation characteristics and partial control by the photosystem II acceptor side. Zeitschrift für Naturforschung C 42, 1246–1254

Oja V., Laisk A. (2020) Time- and reduction-dependent rise of photosystem II fluorescence during microseconds-long inductions in leaves. Photosynthesis Research 145, 209-225

Pospíšil P. (2016) Production of reactive oxygen species by photosystem II as a response to light and temperature stress. Frontiers in Plant Science 7, 1950

Rascher U., Nedbal L. (2006) Dynamics of phtosynthesis in fluctuating light. Current Opinion in Plant Biology 9, 671-678

Reid W.T. (1972) Riccati differential equations. Elsevier

Ruban A.V. (2016) Nonphotochemical chlorophyll fluorescence quenching: mechanism and effectiveness in protecting plants from photodamage. Plant Physiology 170, 1903-1916

Samson G., Bonin L., Maire V. (2019) Dynamics of regulated YNPQ and non-regulated YNO energy dissipation in sunflower leaves exposed to sinusoidal lights. Photosynthesis Research 141, 315–330

Schwartz L. (2008) Mathematics for the physical sciences. Courier Dover Publications

Schansker G., TÓth S.Z., Kovács L., Holzwarth A.R., Garab G. (2011) Evidence for a fluorescence yield change driven by a light induced conformational change within photosystem II during the fast chlorophyll a fluorescence rise. Biochimica et Biophysica Acta - Bioenergetics 1807, 1032-1043

Shimakawa G., Miyake C. (2018) Changing frequency of fluctuating light reveals the molecular mechanism for P700 oxidation in plant leaves. Plant Direct. 2, 73

Singsaas E.L., Sharkey T.D. (1998) The regulation of isoprene emission responses to rapid leaf temperature fluctuations. Plant Cell Environment 21, 1181-1188

Sipka G., Magyar M., Mezzetti A., Akhtar P., Zhu Q., Xiao Y., Han G., Santabarbara S., Shen J.-R., Lambrev P.H., Garab G. (2021) Light-adapted charge-separated state of photosystem II: structural and functional dynamics of the closed reaction center. Plant Cell, in press, doi: 10.1093/plcell/koab008

Sivak M.N., Walker D.A. (1985) Chlorophyll *a* fluorescence: can it shed light on fundamental questions in photosynthetic carbon dioxide fixation? Plant Cell and Environment 8 439-448

Sivak M.N., Walker D.A. (1986) Photosynthesis *in vivo* can be limited by phosphate supply. New Phytologist 102, 499-512

Sivak M.N., Walker D.A. (1987) Oscillations and other symptoms of limitation of *in vivo* photosynthesis by inadequate phosphate supply to the chloroplast. Plant Physiology and Biochemistry 25, 635-648

Slattery R.A., Walker B.J., Weber A.P.M., Ort D.R. (2018) The impacts of fluctuating light on crop performance. Plant Physiology 176, 990-1003

Stirbet A., Lazár D., Guo Y., Govindjee G. (2020) Photosynthesis: basics, history and modelling. Annals of Botany 126, 511-537

Stirbet A., Lazár D., Kromdijk J., Govindjee (2018) Chlorophyll *a* fluorescence induction: Can just a one-second measurement be used to quantify abiotic stress responses? Photosynthetica 56, 86-104

Strasser R.J., Govindjee (1991) The F_0 and the O–J–I–P fluorescence rise in higher plants and algae. In: Regulation of Chloroplast Biogenesis (Argyroudi-Akoyunoglou J.H., ed.), pp. 423-426. Plenum Press, New York

Suga M, Akita F., Sugahara M. et al. (2017) Light-induced structural changes and the site of O=O bond formation in PSII caught by XFEL. Nature 543, 131-135

Tikhonov A.N. (2015) Induction events and short-term regulation of electron transport in chloroplasts: an overview. Photosynthesis Research 125, 65-94

Trtílek M. Kramer D.M., Koblížek M., Nedbal L. (1997) Dual-modulation LED kinetic fluorometer. Journal of Luminescence 72-74, 597-599

van Amerongen H, Chmelinov J. (2020) Instantenous switching between different modes of non-photochemical quanching in plants. Coensequences of inctreasing biomass production. Biochimica et Biophysica Acta – Bionergetics 1861, 148119

van Kooten O., Snel J.F.H., Vredenberg W.J. (1986) Photosynthetic free energy transduction related to the electric potential changes across the thylakoid membrane. Photosynthesis Research 9, 211-227

Vialet-Chabrand S., Matthews J.S.A., Simkin A.J., Raines C.A., Lawson T. (2017) Importance of fluctuations in light on plant photosynthetic acclimation. Plant Physiology 173, 2163-2179

Walker D.A., Sivak M.A., Prinsley R.T., Cheesborough J.K. (1983) Simultaneous measurement of oscillations in oxygen evolution and chlorophyll *a* fluorescence in leaf pieces. Plant Physiology 73, 542-549

Walker D.A., Sivak M.N. (1985) Can phosphate limit photosynthetic carbon assimilation *in vivo*? Physiolgie Végétale 23, 829-841

Wang Y., Burgess S.J., de Becker E.M., Long S.P. (2020) Photosynthesis in the fleeting shadows: an overlooked opportunity for increasing crop productivity? Plant Journal 101, 874-884

Supplementary Materials

Photosynthesis dynamics and regulation sensed in the frequency domain

Ladislav Nedbal[1] and Dušan Lazár[2]

[1] Institute of Bio- and Geosciences/Plant Sciences (IBG-2), Forschungszentrum Jülich, Wilhelm-Johnen-Straße, D-52428 Jülich, Germany

[2] Department of Biophysics, Centre of the Region Haná for Biotechnological and Agricultural Research, Palacký University Olomouc, Šlechtitelů 27, 783 71 Olomouc, Czech Republic

Supplementary Materials consist of:

SM1. Results supplementing Fig. 6 in the main text

SM2. Essentials for dynamic analysis of photosynthesis in harmonically modulated light

SM3. Heuristic exploitation of time- and frequency-domain approaches in physics and engineering

SM4. Analytical solutions of the simplified model of photosynthetic regulation.

References

SM1. Results supplementing Fig. 6 in the main text

The model (Lazár 2009) leads to the prediction (Fig. 6A) that the plastoquinone pool reduction occurring in a low-amplitude light that is modulated with a period of 0.1 s is nearly constant. Statistically around 4.7 plastoquinone molecules out of 5 per photosystem II are predicted to be reduced with very little variation.

The data shown in detail here in the top right panel in Fig. SM1 show that although the model-predicted amplitude is small the dynamics is highly interesting and resembles that seen earlier in higher plants or cyanobacteria (Nedbal and Březina 2002, Nedbal et al. 2003, 2005). The periods of light modulation 10 and 100 ms and 1 s and 10 s are represented by red lines. The amplitude of the modulation was set to produce the same number of photosystem II turnovers as appearing in 20% in the experiments that are reported in the main text.

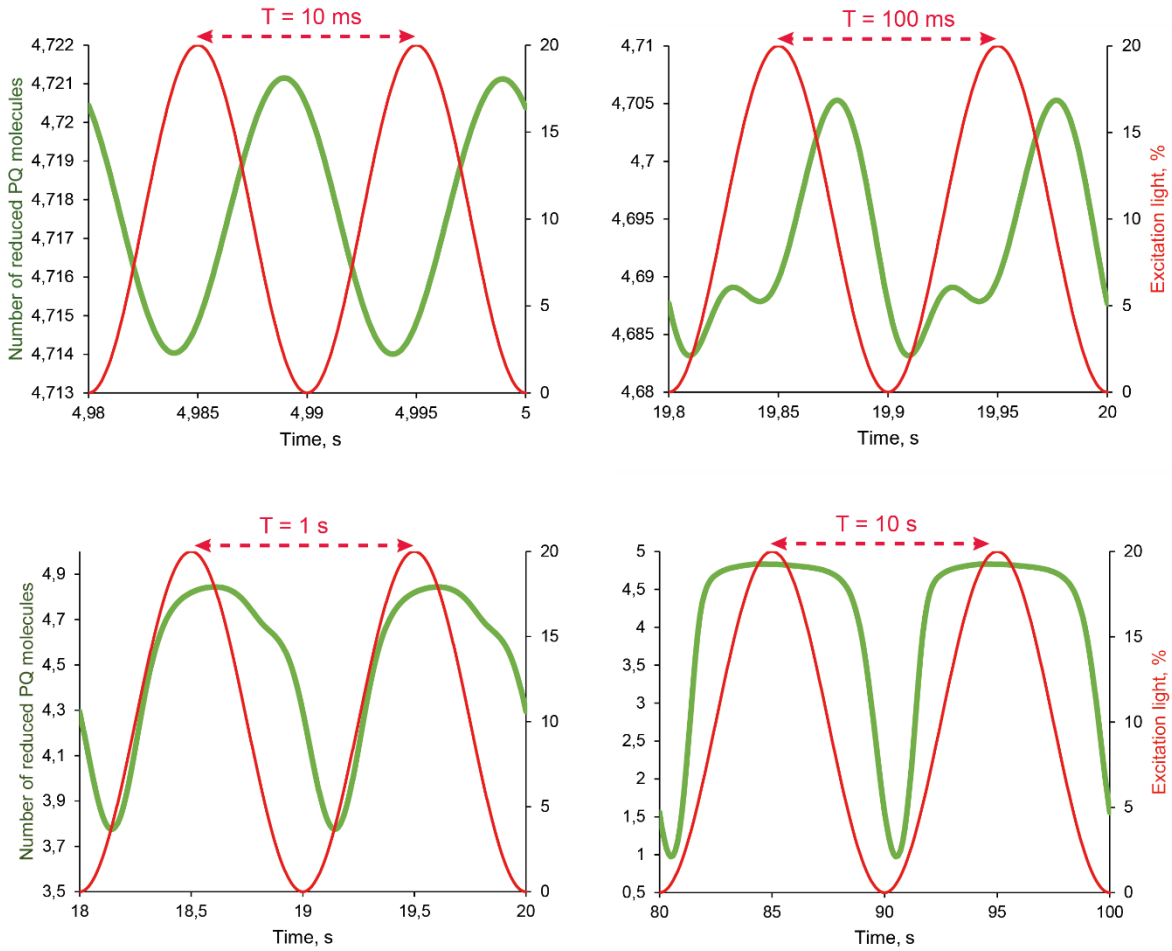

Figure SM1. *The modelled number of reduced plastoquinone molecules per photosystem II is shown by green lines for periods. The light modulation is represented by red lines.*

SM2. Essentials for analysis of photosynthesis in harmonically modulated light

Experimental parameters available for time-domain protocols with dark-to-light transition (blue line) and for the frequency-domain protocols (red line) are schematically depicted in Fig. SM2.

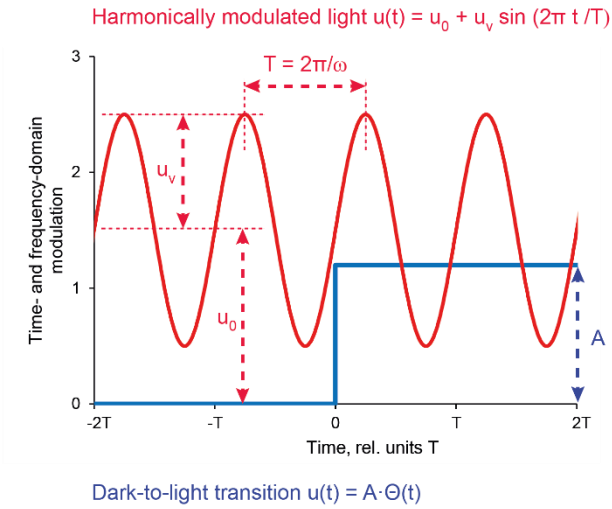

Figure SM2. *The light is modulated as* $A \cdot \Theta(t)$ *(blue line) to measure photosynthetic response to dark-to-light transition in the time domain, where* $\Theta(t)$ *is the Heavyside function. The protocol is fully defined by the amplitude* A*. The protocols for measurements in the frequency domain define oscillating light by its constant level around which the light oscillates,* u_o*, amplitude of the oscillation,* u_v*, and its period, T. In the experiments described in the main text, an equivalent parametrization is also used: light minimum* $u_{min} = u_o - u_v$*, light maximum* $u_{max} = u_o + u_v$*, and angular frequency* $\omega = \frac{2 \cdot \pi}{T}$*.*

The response of photosynthetic modulation to harmonically modulated light can have various forms, e.g., as shown here in Fig. SM1 for reduction of the plastoquinone pool. Relatively simple is the modelled response to light modulated with the period of 10 ms (top left panel in Fig. SM1). Fig. SM3 shows that the response can be well approximated by a single sinusoidal function $PQH_2(t) = \boldsymbol{A_0} + \boldsymbol{A_1} \cdot \mathbf{sin}[\boldsymbol{\omega} \cdot (\boldsymbol{t} - \boldsymbol{\tau_1})]$, where $\boldsymbol{A_0}$ is the constant term in the reduction, $\boldsymbol{A_1}$ is the amplitude of the oscillating term, $\boldsymbol{\omega}$ is the angular frequency of the light modulation, and $\boldsymbol{\tau_1}$ is the phase shift between light modulation and plastoquinone response to the forcing.

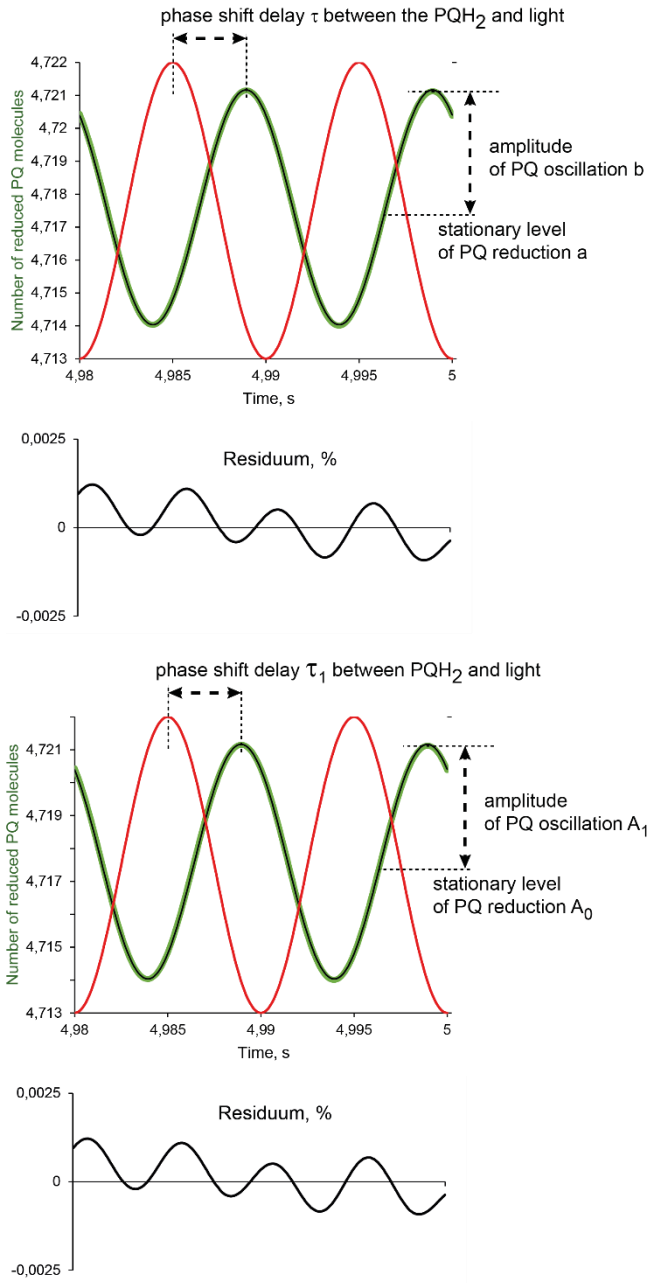

Figure SM3*. Numerical least square fitting of the modelled plastoquinone reduction for T = 10 ms (green line) by* $PQH_2(t) = \boldsymbol{A_0} + \boldsymbol{A_1} \cdot \mathbf{sin}[\boldsymbol{\omega} \cdot (\boldsymbol{t} - \boldsymbol{\tau_1})]$ *(thin black line). The bottom panel shows the residuum, calculated as the relative difference between the fit and the model prediction in %.*

The residuum, i.e. the relative difference between the two curves (top panel in Fig. SM3) remains small within +/- 0.0015% but exhibits an obvious modulation by the first upper harmonic mode that has period $\frac{T}{2}$ and, respectively angular frequency 2ω, where T and ω refer to light modulation period and frequency. The relative difference also drifts, which signals that the model solution was not yet fully stationary/periodic.

Only slightly more complex analysis can be applied to plastoquinone dynamics with light that is modulated with T = 100 ms (Fig. SM4).

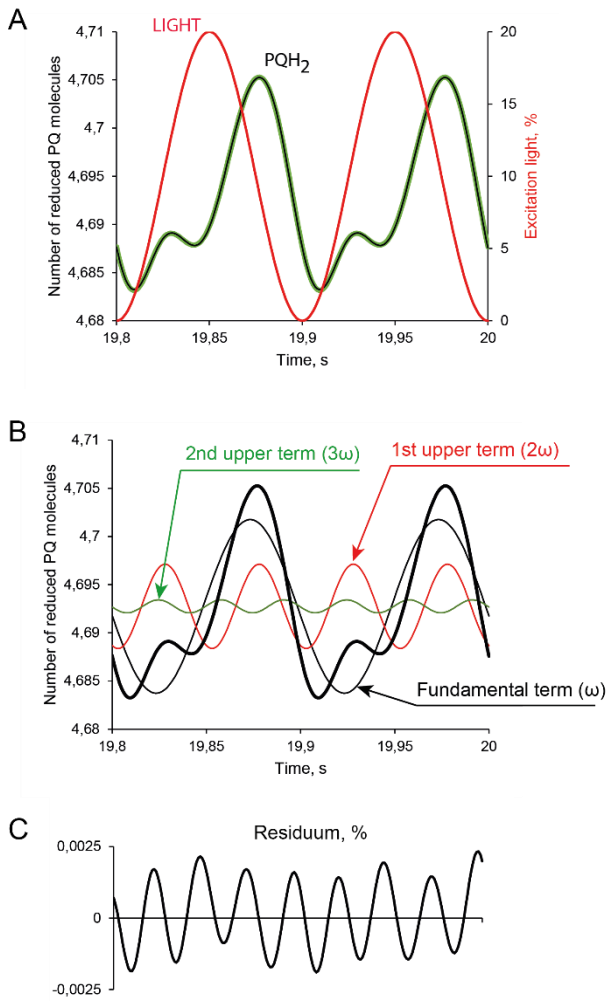

Figure SM4*. Numerical least square fitting of the modelled plastoquinone reduction for T = 100 ms (green line) by* $PQH_2(t) = PQH_2(t) = \boldsymbol{A_0 + A_1 \cdot \sin[\omega \cdot (t - \tau_1)] + A_2 \cdot \sin[2\omega \cdot (t - \tau_2)] + A_3 \cdot \sin[3\omega \cdot (t - \tau_3)]}$ *(thin lines). The bottom panel shows the residuum, calculated as relative difference between the fit and the model prediction in %.*

The residuum in Fig. SM4 after the fitting with fundamental oscillatory term (ω) and with two upper harmonic terms (2ω and 3ω) is very small but not random, exhibiting four pronounced maxima per period and suggesting a tiny contribution of the third upper harmonics (4ω).

The contribution of the third upper harmonic remained negligible also for the period 1 s (not shown) but increased sharply with period of light modulation 10 s. (Fig. SM5).

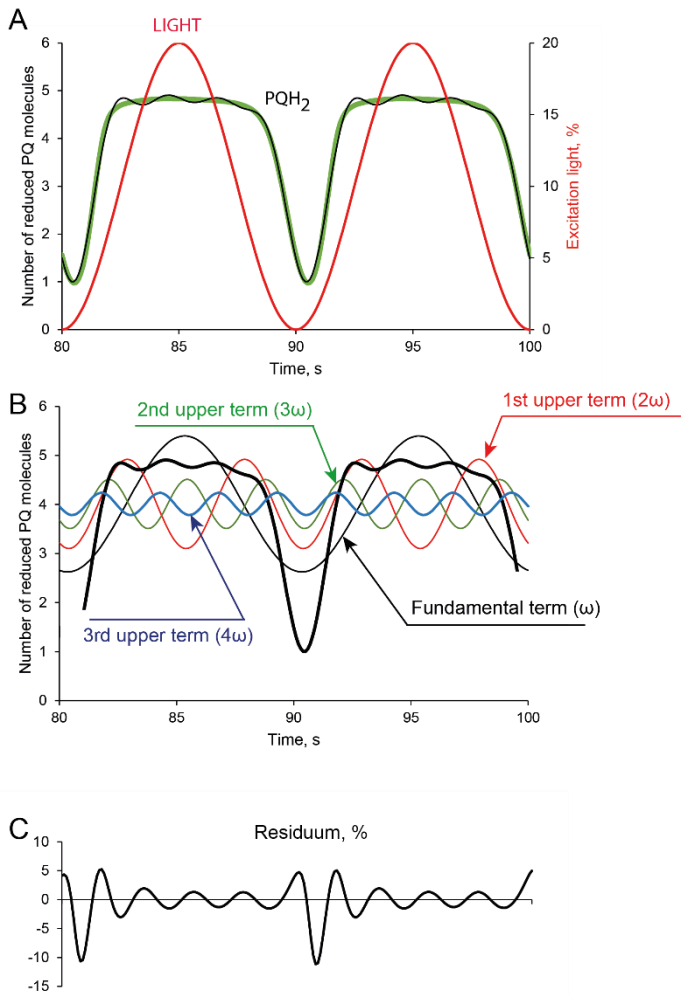

Figure SM5. *Numerical least square fitting of the modelled plastoquinone reduction for T = 10 s (green line) by* $PQH_2(t) = PQH_2(t) = \boldsymbol{A_0} + \boldsymbol{A_1} \cdot \mathbf{sin}[\boldsymbol{\omega} \cdot (\boldsymbol{t} - \boldsymbol{\tau_1})] + \boldsymbol{A_2} \cdot \mathbf{sin}[\boldsymbol{2\omega} \cdot (\boldsymbol{t} - \boldsymbol{\tau_2})] + \boldsymbol{A_3} \cdot \mathbf{sin}[\boldsymbol{3\omega} \cdot (\boldsymbol{t} - \boldsymbol{\tau_3})] + \boldsymbol{A_4} \cdot \mathbf{sin}[\boldsymbol{4\omega} \cdot (\boldsymbol{t} - \boldsymbol{\tau_4})]$ *(thin lines). The bottom panel shows the residuum, calculated as relative difference between the fit and the model prediction in %.*

1

SM3. Heuristic exploitation of time- and frequency-domain approaches in physics and engineering.

The quest for optimal methods to characterize both primary and regulatory processes of photosynthesis that span over many orders of magnitude in time can find inspiration in studies of much simpler systems such as macromolecules in an electric field. The response of macromolecules to electric field includes, similar to photosynthesis, is dictated by multiple factors that act on very different time scales. Upon abrupt application of the electric field, the fastest polarizing are atomic electrons, followed by much slower moving nuclei and, yet, slower moving charged groups of the macromolecules and, in a long-time domain, molecular reorientation can also occur. The resulting polarization of the macromolecular system P(t) to a step-wise change in the electric field E(t)=0 for t<0 and E(t)=E for t≥0 resembles induction of photosynthesis upon sudden exposure of a dark-adapted plant to light:

$$\mathrm{P(t)} = \varepsilon_0 \int_0^t \mathrm{E} \cdot \chi(t-\tau) d\tau \qquad \text{Eq. SM1}$$

The permittivity $\chi(t-\tau)$ function represents all processes that lead to attenuation of the external field by the polarization of the macromolecules $\mathrm{P(t)}$ over all relevant time scales. An identical linear approximation can be suggested for the convolution of photosynthetic processes that occur over many orders of magnitude in time and result in photosynthetic output $\mathrm{P(t)}$. The photosynthesis research can largely benefit from this analogy due to the maturity of formalism that is available for dielectric phenomena that started developing by the pioneering research of Whewell and Faraday already in late 18th century (James 1996). Equation 1 appears in the most convenient form in the frequency domain when the field is not changing abruptly from 0 to E but rather oscillates as a harmonic oscillator $\mathrm{E(t)} = \mathrm{E(\omega)} \cdot \sin(\omega \cdot \mathrm{t})$. Compare with light protocols shown in Fig. SM2.

Using the convolution theorem (Schwartz 2008), one obtains by Fourier transform of integral relation in Eq. SM1 a much simple linear proportionality between the amplitude of field modulation $\mathrm{E(\omega)}$ and the polarization amplitude $\mathrm{P(\omega)}$

$$\mathrm{P(\omega)} = \varepsilon_0 \cdot \chi(\omega) \cdot \mathrm{E(\omega)} \qquad \text{Eq. SM2}$$

where permittivity in the frequency domain $\chi(\omega)$ is obtained by Fourier transform of permittivity in the time-domain $\chi(t)$:

$$\chi(\omega) = \int_{-\infty}^{+\infty} \chi(t) \cdot e^{-i\omega t} \cdot dt \qquad \text{Eq. SM3}$$

The relationship in Eq. SM3 demonstrates that the complex system can be fully characterized in the time domain by $\chi(t)$ or in frequency domain by $\chi(\omega)$ and that both approaches carry equivalent information provided that polarization and electric field are linearly proportional (Eq. SM1).

Per analogy, the same can be true for the relationship between photosynthetic activity probed by oxygen evolution, carbon dioxide uptake or any optical proxy such as Chl fluorescence emission as long as the dynamics occurs in narrow range of linearity. The wealth of information obtained so far in the

time domain in studying dark-to-light transitions or response to light flashes can, thus, be complemented or substituted by studies that are done in the frequency domain by applying harmonically modulated light:

$$\mathrm{PhotosynthesisProxy}(\omega) = \chi(\omega) \cdot \mathrm{Light}(\omega) \qquad \text{Eq. SM4}$$

In this paper, we shall use a simple mathematical model to demonstrate that the approach is valid in the high frequency / low-light domain when the relationship between photosynthesis and light is not affected by regulation and, thus, remains largely linear.

SM4. Analytical solutions with a simplified model of photosynthetic regulation.

Systems theory (von Bertalanffy 1993) is exploring and exploiting homologies between complex systems, similar to those shortly described in SM3. Many of these homologies are appearing only at higher levels of the system hierarchy and may not be apparent in detailed molecular models such as those used in the main text (Lazár 2009). Sometimes can be dynamic behavior described by analytically solvable equation connecting systemic inputs and observables. In case of photosynthesis, this can be attempted by a dramatic simplification, which would lead to reduction of model complexity to light as the single input and a small number of system variables, such as linear electron transport between the photosystems that is coupled to transport of protons across the thylakoid membrane. The regulation of photosystem II antenna can then be approximated as being proportional to the proton concentration difference across the thylakoid membrane. This simplified model (Fig. SM6) deviates from the modelled photosynthetic processes in several key features, e.g.: it does not consider cyclic electron flow, it does not distinguish electric and chemical terms of the potential difference across the membrane and is based on several other crude simplifications that are described below in detail. Nevertheless, we show here that such a simplified, analytically solvable model can demonstrate that the upper harmonic modulation observed in long periods of weak light (Fig. 1C) appear as a direct consequence of regulation.

<u>*SUMMARY OF THE DETAILED CALCULATIONS BELOW:*</u>

The *zero-level approximation* $\Psi_0(t)$ that is calculated for unregulated system ($\delta(t) = \Delta = 0$) leads to model prediction:

$$\Psi_0(t) = \frac{u_0}{\alpha \cdot \beta} + \frac{u_V}{\alpha} \cdot \left[\frac{\beta}{\beta^2+\omega^2} \cdot \sin(\omega \cdot t) - \frac{\omega}{\beta^2+\omega^2} \cdot \cos(\omega \cdot t)\right] \qquad \text{Eq.SM24a BELOW}$$

The variable part $\Phi_0(t) = \Psi_0(t) - \frac{u_0}{\alpha \cdot \beta}$ is:

$$\Phi_0(t) = \frac{u_V}{\alpha} \cdot \left[\frac{\beta}{\beta^2+\omega^2} \cdot \sin(\omega \cdot t) - \frac{\omega}{\beta^2+\omega^2} \cdot \cos(\omega \cdot t)\right].$$

This solution predicts that the potential will be modulated, in absence of regulation, as simple sinus and thus without any harmonics.

The equation in the first level approximation of regulation Δ is derived for the variable potential:

$$\Phi(t) \approx \Phi_0(t) + \Delta \cdot \Phi_1(t) \qquad \text{Eq. SM27 BELOW}$$

assuming that the photosystem II antenna has a variable component $\sigma_{\mathrm{II},v}(t)$ that is controlled by the deviation of the potential $\Psi(t)$ from its steady-state value $\frac{u_0}{\alpha\beta}$:

$$\sigma_{\mathrm{II},v}(t) = s \cdot \left(\Psi(t) - \frac{u_0}{\alpha\beta}\right) \qquad \text{Eq. SM25a BELOW}$$

and $\Delta = \frac{s}{2\sigma}$ and $\frac{\sigma_{\mathrm{II},v}(t)}{2\sigma} = \delta(t)$ (in Fig.3).

The first Taylor term of the variable part of the electrochemical potential across the thylakoid membrane $\Phi_1(t)$ in Eq. 40 relates to the the total variable part by Eq. SM27:

$$\Phi(t) \approx \Phi_0(t) + \Delta \cdot \Phi_1(t) \qquad \text{Eq.SM27 BELOW}$$

Where $\Phi_0(t)$ is corresponding to the solution of Eq. SM18 for $\delta(t) = \Delta = 0$.

$\Phi_1(t) = \varphi_1(t) \cdot e^{-\beta \cdot t}$ is obtained by integration of Eq. SM38 and appears in form presented in Eq. SM41. The Eq. SM41 can be rearranged into several equivalent forms that, however, always suggest components that are modulated by fundamental frequency of the light modulation ωt and first upper harmonic modulation of $2\omega t$. The same can be concluded for $\Psi(t)$ which leads to Eq. 5 of the main text:

$$\Psi_1(t) = A(\omega, \alpha, \beta, u_0, u_v) \cdot sin(\omega \cdot (t - \tau_A(\omega, \alpha, \beta, u_0, u_v)) + \boldsymbol{B(\omega, \alpha, \beta, u_0, u_v)} \cdot \boldsymbol{sin(2 \cdot \omega \cdot (t - \tau_B(\omega, \alpha, \beta, u_0, u_v))} \qquad \text{Eq. 5 REPEATED}$$

With the potential $\Psi(t)$ including the zero-level $\Psi_0(t)$ and the first level $\Psi_1(t)$ approximations:

$$\Psi(t) \approx \Psi_0(t) + \Delta \cdot \Psi_1(t) + \cdots$$

and with $\Psi_0(t)$ that is modulated only by the fundamental mode $\omega \cdot t$ the calculations confirm that **<u>the upper harmonic modulation will occur, according to the model, only for regulation $\Delta \neq 0$.</u>**

This was derived for one, very simplified model but similar considerations can be applied for other models, in which systems variables occur in their equation in products with the light or/and in squares as it is the case in the Ricatti equation (Eq. 4) in the main text and in Eq. SM25a-c.

DETAILED CALCULATIONS:

The incident light is harmonically modulated (see also Fig. SM2):

$$u(t) = u_0 + u_V \cdot \sin(\omega \cdot t), \qquad \text{Eq. SM5}$$

where $u_V \geq u_0$.

The core drivers in primary photosynthesis are the two photosystems (Fig. SM6) that can be seen as two serially operating pumps driven by the periodic input with a pool that is filled by Pump II (*"push"*) and emptied by Pump I (*"pull"*). The pool content would be characterized by the state variable x(t) (reduction of the plastoquinone pool, Fig. SM1).

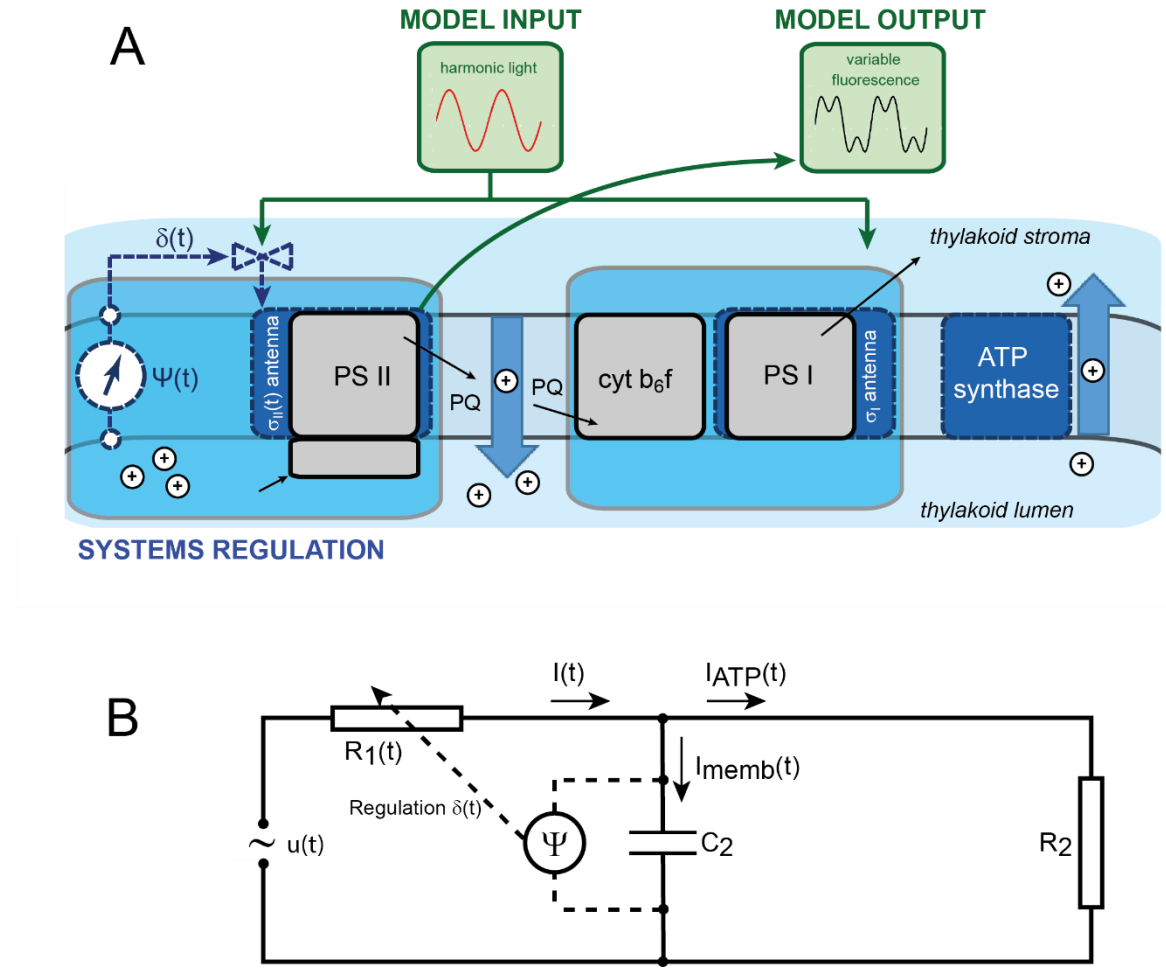

Figure SM6. *Simplified model of photosynthetic antenna regulation (A) and model-equivalent electrical circuit (B).*

Flow into the pool is supposed to be regulated, with $\sigma_{II,v}(t)$ dependent on the state variables:

$$\frac{dx_{in}(t)}{dt} = u(t) \cdot \sigma_{II}(t) = (u_0 + u_V(t)) \cdot \left(\sigma_{II,0} - \sigma_{II,v}(t)\right) \quad \text{Eq. SM6}$$

Flow out of the pool is supposed not to be regulated, with $\sigma_{I,0}$ constant:

$$\frac{dx_{out}(t)}{dt} = -u(t) \cdot \sigma_{I,0} = -(u_0 + u_V(t)) \cdot \sigma_{I,0} \quad \text{Eq. SM7}$$

In a stationary limit $u_V(t) = 0, \sigma_{II,v}(t) = 0, \frac{dx(t\to\infty)}{dt} = \frac{d[x_{in}(t\to\infty)+x_{out}(t\to\infty)]}{dt} = I_0 \cdot \left(\sigma_{II,0} - \sigma_{I,0}\right) = 0,$ which leads to $\sigma_{II,0} = \sigma_{I,0} = \sigma$, transforming Eq. SM7 to Eq. SM8.

$$\frac{dx(t)}{dt} = \frac{d[x_{in}(t)+x_{out}(t)]}{dt} = u(t) \cdot (\sigma_{II}(t) - \sigma_I) = (u_0 + u_V(t)) \cdot \sigma_{II,v}(t) \quad \text{Eq. SM8}$$

The flow of electrons $\frac{dx(t)}{dt}$ in Eq. SM8 is assumed in the simplified model to be coupled to the flow of protons (symbol I) across the membrane associated with photosystem II: $\mathrm{I}_{PSII}(t) = \xi \cdot \frac{dx_{in}(t)}{dt} = (u_0 + u_V(t)) \cdot \xi \cdot \left(\sigma - \sigma_{II,v}(t)\right)$ and the flow of protons I across the membrane associated with cytochrome b_6/f and photosystem I: $\mathrm{I}_{PSI}(t) = \xi \cdot \frac{-dx_{out}(t)}{dt} = \xi \cdot \frac{-dx_{out}(t)}{dt} = (u_0 + u_V(t)) \cdot \xi \cdot \sigma$, where ξ is the stoichiometry of coupling between electron and proton transport (for simplicity assumed to be the same for photosystem II and photosystem I).

The total flow of protons associated with functioning of the two photosystems is then modeled as:

$$I(t) = \mathrm{I}_{PSII}(t) + \mathrm{I}_{PSI}(t) = (u_0 + u_V(t)) \cdot \xi \cdot \left(2\sigma - \sigma_{II,v}(t)\right) \quad \text{Eq. SM9}$$

and results in a buildup of the potential across the membrane

$$\Psi(t) = \frac{1}{C} \cdot \left[Q_0 + \int_0^t I_{memb}(\tau) d\tau\right] \quad \text{Eq. SM10}$$

where C is the capacitance of the membrane, $I_{memb} = I - I_{ATP}(\tau)$ and $I_{ATP}(\tau) = \Psi(t)/R_2$ is the counterflow of protons that drives the ATP-synthase, R_2 is characterizing the ATP-ase 'resistance'. Relabeling $\frac{1}{R_1(t)} = \xi \cdot \left(2\sigma - \sigma_{II,v}(t)\right)$, one can see the model system as homologous to the simple electronic circuit shown in Fig. SM6B.

The potential difference across the membrane and that driving the ATP-synthase are the same:

$$\Psi(t) = \frac{1}{C} \cdot \left[Q_0 + \int_0^t I_{memb}(\tau) d\tau\right] = R_2 \cdot I_{ATP}(t) \quad \text{Eq. SM11}$$

yielding the ATP-synthase flux:

$$I_{ATP}(t) = \frac{1}{R_2 \cdot C} \cdot \left[Q_0 + \int_0^t I_{memb}(\tau) d\tau\right] \quad \text{Eq. SM12}$$

With this, the Ohm law gives:

$$\mathrm{u}(t) = R_1(t) \cdot I_{memb}(t) + \frac{R_1(t)+R_2}{R_2 \cdot C} \cdot \left[Q_0 + \int_0^t I_{memb}(\tau) d\tau\right] \quad \text{Eq. SM13}$$

Equation SM13 connects the flux of protons driven by the two photosystems $I_{memb}(t)$ to light $\mathrm{u}(t)$ with parameters $R_1(t)$, R_2, C, and Q_0. Combining Eqs. SM13 and SM5, one obtains:

$$u_0 + u_V \cdot \sin(\omega \cdot t) = R_1(t) \cdot I_{memb}(t) + \frac{R_1(t)+R_2}{R_2 \cdot C} \cdot \left[Q_0 + \int_0^t I_{memb}(\tau) d\tau\right] \quad \text{Eq. SM14}$$

Using Eq. SM10, one can reformulate Eq. SM14 to calculate electrochemical potential difference across the membrane:

$$u_0 + u_V \cdot \sin(\omega \cdot t) = R_1(t) \cdot C \cdot \frac{d\Psi(t)}{dt} + \frac{R_1(t)}{R_2} \cdot \Psi(t) + \Psi(t) \quad \text{Eq. SM15}$$

$$\frac{1}{R_1(t)} \cdot [u_0 + u_V \cdot \sin(\omega \cdot t) - \Psi(t)] = C \cdot \frac{d\Psi(t)}{dt} + \frac{1}{R_2} \cdot \Psi(t) \quad \text{Eq. SM16}$$

where constant and variable parts can be separated: $\frac{1}{R_1(t)} \equiv \frac{1}{R_1} - \frac{1}{R_v(t)}$ with $\frac{1}{R_1} = \xi \cdot 2\sigma$ and $\frac{1}{R_v(t)} = \xi \cdot \sigma_{\mathrm{II},v}(t)$ corresponding to the unregulated and regulated proton flows.

$$\left(\frac{1}{R_1} - \frac{1}{R_v(t)}\right) \cdot [u_0 + u_V \cdot \sin(\omega \cdot t) - \Psi(t)] = C \cdot \frac{d\Psi(t)}{dt} + \frac{1}{R_2} \cdot \Psi(t) \quad \text{Eq. SM17}$$

Introducing new parameters $\alpha = R_1 \cdot C$, $\beta = \frac{1}{C} \cdot \left(\frac{1}{R_2} + \frac{1}{R_1}\right)$, $\delta(t) = \frac{R_1}{R_v(t)} = \frac{\sigma_{\mathrm{II},v}(t)}{2\sigma}$, Eq. SM17 can be reformulated to:

$$(u_0 + u_V \cdot \sin(\omega \cdot t)) - \alpha \cdot \left(\frac{d\Psi(t)}{dt} + \beta \cdot \Psi(t)\right) = \delta(t) \cdot [u_0 + u_V \cdot \sin(\omega \cdot t) - \Psi(t)]$$

Eq. SM18

The left side of Eq. SM18 contains exclusively terms that are independent of regulation and the right side is proportional to $\delta(t) = \frac{\sigma_{\mathrm{II},v}(t)}{2\sigma}$, which is the ratio of regulated and unregulated antenna.

Analytical solution of the model equation for an unregulated system ($\delta = 0$)

In the case of no regulation ($\delta = 0$), the left side of Eq. SM18 is zero and the electrochemical potential $\Psi_0(t)$ is expected to be simulated by Eq. SM19:

$$(u_0 + u_V \cdot \sin(\omega \cdot t)) - \alpha \cdot \left(\frac{d\Psi_0(t)}{dt} + \beta \cdot \Psi_0(t)\right) = 0 \quad \text{Eq. SM19}$$

Using the substitution $\Psi_0(t) = \varphi_0(t) \cdot e^{-\beta \cdot t}$, the Eq. SM19 takes the following form:

$$\frac{d\varphi_0(t)}{dt} = \left(\frac{u_0}{\alpha} + \frac{u_V}{\alpha} \cdot \sin(\omega \cdot t)\right) \cdot e^{\beta \cdot t} \quad \text{Eq. SM20}$$

Converting the right side of Eq. 20 to a purely exponential form, one obtains:

$$\frac{d\varphi_0(t)}{dt} = \frac{u_0}{\alpha} \cdot e^{\beta \cdot t} + \frac{u_V}{\alpha} \cdot \frac{e^{(\beta+i\omega)t} - e^{(\beta-i\omega)t}}{2i} \qquad \text{Eq. SM21}$$

The Eq. 21 can be easily integrated yielding:

$$\varphi_0(t) - \varphi_{00} = \frac{u_0}{\alpha \cdot \beta} \cdot e^{\beta \cdot t} + \frac{u_V}{2i \cdot \alpha} \cdot \left(\frac{e^{(\beta+i\omega)t}}{\beta+i\omega} - \frac{e^{(\beta-i\omega)t}}{\beta-i\omega}\right), \qquad \text{Eq. SM22}$$

where φ_{00} is an integration constant.

Returning from $\varphi_0(t)$ to $\Psi_0(t) = \varphi_0(t) \cdot e^{-\beta \cdot t}$, one obtains:

$$\Psi_0(t) = \varphi_{00} \cdot e^{-\beta \cdot t} + \frac{u_0}{\alpha \cdot \beta} + \frac{u_V}{2i \cdot \alpha} \cdot \left(\frac{e^{+i\omega t}}{\beta+i\omega} - \frac{e^{-i\omega t}}{\beta-i\omega}\right) \qquad \text{Eq. SM23}$$

The integration constant φ_{00} is determined by the intial potential accross the membrane $\varphi_{00} = \Psi_0(t=0) - \frac{u_0}{\alpha \cdot \beta} + \frac{u_V}{\alpha} \cdot \frac{\omega}{\beta^2+\omega^2}$.

$$\Psi_0(t) = (\Psi_0(0) - \frac{u_0}{\alpha \cdot \beta} + \frac{u_V}{\alpha} \cdot \frac{\omega}{\beta^2+\omega^2}) \cdot e^{-\beta \cdot t} + \frac{u_0}{\alpha \cdot \beta} + \frac{u_V}{2i \cdot \alpha} \cdot \left(\frac{e^{+i\omega t}}{\beta+i\omega} - \frac{e^{-i\omega t}}{\beta-i\omega}\right) \qquad \text{Eq. SM23a}$$

or, expressed in trigonometric functions:

$$\Psi_0(t) = (\Psi_0(0) - \frac{u_0}{\alpha \cdot \beta} + \frac{u_V}{\alpha} \cdot \frac{\omega}{\beta^2+\omega^2}) \cdot e^{-\beta \cdot t} + \frac{u_0}{\alpha \cdot \beta} + \frac{u_V}{\alpha} \cdot [\frac{\beta}{\beta^2+\omega^2} \cdot \sin(\omega \cdot t) - \frac{\omega}{\beta^2+\omega^2} \cdot \cos(\omega \cdot t)]. \qquad \text{Eq. SM24}$$

Considering that only stationary oscillations in the long time limit are of interest one can neglect the initial transient and use only:

$$\Psi_0(t) = \frac{u_0}{\alpha \cdot \beta} + \frac{u_V}{\alpha} \cdot [\frac{\beta}{\beta^2+\omega^2} \cdot \sin(\omega \cdot t) - \frac{\omega}{\beta^2+\omega^2} \cdot \cos(\omega \cdot t)]. \qquad \text{Eq. SM24a}$$

The formal analogy with the dielectric permittivity mentioned in the introductory paragraphs and in SM3 is visible also in Eq. SM24 that is homologous to the Debye equations for ideal, non-interacting population of dipoles in an alternating external electric field (Debye 1913).

Using trivial trigonometric formulae, Eq. SM24a can be also expressed in an equivalent form:

$$\boldsymbol{\Psi_0(t) = \frac{u_0}{\alpha \cdot \beta} + \frac{u_V}{\alpha} \cdot \left[\frac{1}{\sqrt{\beta^2+\omega^2}} \cdot sin\left(\omega \cdot t - arccos\frac{\beta}{\sqrt{\beta^2+\omega^2}}\right)\right]} \qquad \text{Eq. SM24b}$$

<u>This form is used in Eq. 3 of the main text.</u>

Analytical solution of the model equation for a weakly regulated system ($0 < \delta \ll 1$)

The general equation of the model that includes regulation was formulated in Eq. SM18:

$$(u_0 + u_V \cdot \sin(\omega \cdot t)) - \alpha \cdot \left(\frac{d\Psi(t)}{dt} + \beta \cdot \Psi(t)\right) = \delta(t) \cdot [u_0 + u_V \cdot \sin(\omega \cdot t) - \Psi(t)],$$

REPEATED Eq.SM18

where $\delta(t)$ represents the relative variation of the effective antenna size $\frac{\sigma_{\mathrm{II},v}(t)}{2\sigma}$ of photosystem II that is caused by the regulation. In one physiologically meaningful scenario, one can assume that that the antenna is reduced by regulation when the electrochemical potential deviates from the steady state $\frac{u_0}{\alpha\beta}$ that is established in constant irradiance u_0 and that the reduction is linearly proportional to the deviation from homeostasis $\left(\Psi(t) - \frac{u_0}{\alpha\beta}\right)$:

$$\sigma_{\mathrm{II},v}(t) = s \cdot \left(\Psi(t) - \frac{u_0}{\alpha\beta}\right), \qquad \text{Eq. SM25a}$$

where s is a constant of the linear proportionality. The relative variation of the effective antenna size can, with this approximation, be formulated as:

$$\delta(t) = \frac{\sigma_{\mathrm{II},v}(t)}{2\sigma} = \frac{s}{2\sigma} \cdot \left(\Psi(t) - \frac{u_0}{\alpha\beta}\right) \qquad \text{Eq. SM25b}$$

Mathematically convenient is to formulate the equations for the deviation of the potential $\Psi(t)$ from homeostasis $\Phi(t) = \Psi(t) - \frac{u_0}{\alpha\beta}$ and to introduce a new regulation parameter $\Delta = \frac{s}{2\sigma}$:

$$\delta(t) = \frac{s}{2\sigma} \cdot \Phi(t) = \Delta \cdot \Phi(t). \qquad \text{Eq. SM25c}$$

With this, Eq.SM18 takes the following form:

$$u_V \cdot \sin(\omega \cdot t) - \alpha \cdot \left(\frac{d\Phi(t)}{dt} + \beta \cdot \Phi(t)\right) = \Delta \cdot \Phi(t) \cdot \left[u_0 \cdot \left(1 - \frac{1}{\alpha\beta}\right) + u_V \cdot \sin(\omega \cdot t) - \Phi(t)\right].$$

Eq. SM26

<u>This is the form that is presented in Eq. 4 of the main text.</u>

Assuming that the requlation is weak, $\Delta \ll 1$, one can approximate the solution of Eq. SM26 by the the zero and first order terms of Taylor series in Δ:

$$\Phi(t) \approx \Phi_0(t) + \Delta \cdot \Phi_1(t), \qquad \text{Eq. SM27}$$

where $\Phi_0(t)$ is corresponding to the solution of Eq. SM18 for $\delta(t) = \Delta = 0$.

In this approximation, the Eq. 26b takes the following new form:

$$u_V \cdot \sin(\omega \cdot t) - \alpha \cdot (\frac{d(\Phi_0(t)+\Delta\cdot\Phi_1(t))}{dt} + \beta \cdot (\Phi_0(t) + \Delta \cdot \Phi_1(t))) \approx \Delta \cdot (\Phi_0(t) + \Delta \cdot \Phi_1(t)) \cdot \left[u_0 \cdot (1 - \frac{1}{\alpha\beta}) + u_V \cdot \sin(\omega \cdot t) - (\Phi_0(t) + \Delta \cdot \Phi_1(t))\right] \quad \text{Eq. SM28}$$

and:

$$u_V \cdot \sin(\omega \cdot t) - \alpha \cdot \left(\frac{d\Phi_0(t)}{dt} + \beta \cdot \Phi_0(t)\right) - \alpha \cdot \Delta \cdot \left(\frac{d\Phi_1(t)}{dt} + \beta \cdot \Phi_1(t)\right) \approx \Delta \cdot \Phi_0(t) \cdot \left[u_0 \cdot \left(1 - \frac{1}{\alpha\beta}\right) + u_V \cdot \sin(\omega \cdot t) - \Phi_0(t) - \Delta \cdot \Phi_1(t)\right] + \Delta^2 \cdot \Phi_1(t) \cdot \left[u_0 \cdot \left(1 - \frac{1}{\alpha\beta}\right) + u_V \cdot \sin(\omega \cdot t) - \left(\Phi_0(t) + \Delta \cdot \Phi_1(t)\right)\right]. \quad \text{Eq. SM29}$$

By neglecting in Eq. SM29 all the terms that are proportional to Δ^2, one obtains:

$$u_V \cdot \sin(\omega \cdot t) - \alpha \cdot \left(\frac{d\Phi_0(t)}{dt} + \beta \cdot \Phi_0(t)\right) \approx \alpha \cdot \Delta \cdot \left(\frac{d\Phi_1(t)}{dt} + \beta \cdot \Phi_1(t)\right) + \Delta \cdot \Phi_0(t) \cdot \left[u_0 \cdot \left(1 - \frac{1}{\alpha\beta}\right) + u_V \cdot \sin(\omega \cdot t) - \Phi_0(t)\right]. \quad \text{Eq. SM30a}$$

The left side of Eq. SM30a is zero because:

$$u_V \cdot \sin(\omega \cdot t) - \alpha \cdot \left(\frac{d\Phi_0(t)}{dt} + \beta \cdot \Phi_0(t)\right) = u_V \cdot \sin(\omega \cdot t) - \alpha \cdot \left(\frac{d\Psi_0(t)}{dt} + \beta \cdot (\Psi_0(t) - \frac{u_0}{\alpha\beta})\right) = u_0 + u_V \cdot \sin(\omega \cdot t) - \alpha \cdot \left(\frac{d\Psi_0(t)}{dt} + \beta \cdot \Psi_0(t)\right), \quad \text{Eq. SM30b}$$

where the right side of Eq.30b is zero because of Eq. SM19.

With this:

$$0 \approx \alpha \cdot \Delta \cdot \left(\frac{d\Phi_1(t)}{dt} + \beta \cdot \Phi_1(t)\right) + \Delta \cdot \Phi_0(t) \cdot \left[u_0 \cdot \left(1 - \frac{1}{\alpha\beta}\right) + u_V \cdot \sin(\omega \cdot t) - \Phi_0(t)\right]. \quad \text{Eq. SM31}$$

Using another substitution $\Phi_1(t) = \varphi_1(t) \cdot e^{-\beta \cdot t}$, one obtains:

$$\frac{d\varphi_1(t)}{dt} \approx -\frac{1}{\alpha} \cdot \Phi_0(t) \cdot e^{\beta \cdot t} \cdot \left[u_0 \cdot \left(1 - \frac{1}{\alpha\beta}\right) + u_V \cdot \sin(\omega \cdot t) - \Phi_0(t)\right] \quad \text{Eq. SM32a}$$

or

$$\frac{d\varphi_1(t)}{dt} \approx -\frac{u_0 \cdot \left(1 - \frac{1}{\alpha\beta}\right)}{\alpha} \cdot \Phi_0(t) \cdot e^{\beta \cdot t} - \frac{u_V}{\alpha} \cdot \Phi_0(t) \cdot e^{\beta \cdot t} \cdot \sin(\omega \cdot t) + \frac{1}{\alpha} \cdot \Phi_0(t)^2 \cdot e^{\beta \cdot t}. \quad \text{Eq. SM32b}$$

Using the zero-approximation solution derived above, $\Phi_0(t) = \frac{u_V}{2i \cdot \alpha} \cdot \left(\frac{e^{+i\omega t}}{\beta + i\omega} - \frac{e^{-i\omega t}}{\beta - i\omega}\right)$, one obtains for the first term in Eq. SM32b:

$$-\frac{u_0\cdot\left(1-\frac{1}{\alpha\beta}\right)}{\alpha}\cdot\Phi_0(t)\cdot e^{\beta\cdot t}=-\frac{u_0\cdot\left(1-\frac{1}{\alpha\beta}\right)}{\alpha}\cdot\frac{u_V}{2i\cdot\alpha}\cdot\left(\frac{e^{+i\omega t}}{\beta+i\omega}-\frac{e^{-i\omega t}}{\beta-i\omega}\right)\cdot e^{\beta\cdot t} \qquad \text{Eq. SM33a}$$

$$-\frac{u_0\cdot\left(1-\frac{1}{\alpha\beta}\right)}{\alpha}\cdot\Phi_0(t)\cdot e^{\beta\cdot t}=-e^{\beta t}\cdot\frac{u_0\cdot u_v\cdot\left(1-\frac{1}{\alpha\beta}\right)}{2i\cdot\alpha^2}\cdot\left(\frac{e^{i\omega t}}{\beta+i\omega}-\frac{e^{-i\omega t}}{\beta-i\omega}\right) \qquad \text{Eq. SM33c}$$

$$-\frac{u_0\cdot\left(1-\frac{1}{\alpha\beta}\right)}{\alpha}\cdot\Phi_0(t)\cdot e^{\beta\cdot t}=-e^{\beta t}\cdot\frac{u_0\cdot u_v\cdot\left(1-\frac{1}{\alpha\beta}\right)}{2i\cdot\alpha^2(\beta+i\omega)}\cdot e^{i\omega t}+e^{\beta t}\cdot\frac{u_0\cdot u_v\cdot\left(1-\frac{1}{\alpha\beta}\right)}{2i\cdot\alpha^2(\beta-i\omega)}\cdot e^{-i\omega t}. \qquad \text{Eq. SM33d}$$

The second term in Eq. SM32b:

$$-\frac{u_V}{\alpha}\cdot\Phi_0(t)\cdot e^{\beta\cdot t}\cdot\sin(\omega\cdot t)=-e^{\beta t}\cdot\left(\frac{u_V}{2\alpha}\right)^2\cdot\frac{2\beta}{\beta^2+\omega^2}+e^{\beta t}\cdot\left(\frac{u_V}{2\alpha}\right)^2\cdot\frac{1}{\beta+i\omega}\cdot e^{i2\omega t}+e^{\beta t}\cdot\left(\frac{u_V}{2\alpha}\right)^2\cdot\frac{1}{\beta-i\omega}\cdot e^{-i2\omega t}. \qquad \text{Eq. SM34}$$

The third term in Eq. SM32b is then:

$$\frac{1}{\alpha}\cdot\Phi_0(t)^2\cdot e^{\beta\cdot t}=e^{\beta\cdot t}\cdot\frac{1}{\alpha}\cdot\left(\frac{u_V}{2\alpha}\right)^2\cdot\frac{2}{\beta^2+\omega^2}-e^{\beta\cdot t}\cdot\frac{1}{(\beta+i\omega)^2\cdot\alpha}\cdot\left(\frac{u_V}{2\alpha}\right)^2\cdot e^{+i2\omega t}-e^{\beta\cdot t}\cdot\frac{1}{(\beta-i\omega)^2\cdot\alpha}\cdot\left(\frac{u_V}{2\alpha}\right)^2\cdot e^{-i2\omega t}. \qquad \text{Eq. SM35c}$$

Inserting the corresponding terms from Eqs. SM33, SM34, and SM35 in Eq. SM32b yields:

$$\frac{d\varphi_1(t)}{dt}\approx-e^{\beta t}\cdot\frac{u_0\cdot u_v\cdot\left(1-\frac{1}{\alpha\beta}\right)}{2i\cdot\alpha^2(\beta+i\omega)}\cdot e^{i\omega t}+e^{\beta t}\cdot\frac{u_0\cdot u_v\cdot\left(1-\frac{1}{\alpha\beta}\right)}{2i\cdot\alpha^2(\beta-i\omega)}\cdot e^{-i\omega t}-e^{\beta t}\cdot\left(\frac{u_V}{2\alpha}\right)^2\cdot\frac{2\beta}{\beta^2+\omega^2}+e^{\beta t}\cdot\left(\frac{u_V}{2\alpha}\right)^2\cdot\frac{1}{\beta+i\omega}\cdot e^{i2\omega t}+e^{\beta t}\cdot\left(\frac{u_V}{2\alpha}\right)^2\cdot\frac{1}{\beta-i\omega}\cdot e^{-i2\omega t}+e^{\beta\cdot t}\cdot\frac{1}{\alpha}\cdot\left(\frac{u_V}{2\alpha}\right)^2\cdot\frac{2}{\beta^2+\omega^2}-e^{\beta\cdot t}\cdot\frac{1}{(\beta+i\omega)^2\cdot\alpha}\cdot\left(\frac{u_V}{2\alpha}\right)^2\cdot e^{+i2\omega t}-e^{\beta\cdot t}\cdot\frac{1}{(\beta-i\omega)^2\cdot\alpha}\cdot\left(\frac{u_V}{2\alpha}\right)^2\cdot e^{-i2\omega t}. \qquad \text{Eq. SM36}$$

The two constant terms marked by black cancel each other and one obtains:

$$\frac{d\varphi_1(t)}{dt}\approx-e^{\beta t}\cdot\frac{u_0\cdot u_v\cdot\left(1-\frac{1}{\alpha\beta}\right)}{2i\cdot\alpha^2(\beta+i\omega)}\cdot e^{i\omega t}+e^{\beta t}\cdot\frac{u_0\cdot u_v\cdot\left(1-\frac{1}{\alpha\beta}\right)}{2i\cdot\alpha^2(\beta-i\omega)}\cdot e^{-i\omega t}+e^{\beta t}\cdot\left(\frac{u_V}{2\alpha}\right)^2\cdot\frac{1}{\beta+i\omega}\cdot e^{i2\omega t}+e^{\beta t}\cdot\left(\frac{u_V}{2\alpha}\right)^2\cdot\frac{1}{\beta-i\omega}\cdot e^{-i2\omega t}-e^{\beta\cdot t}\cdot\frac{1}{(\beta+i\omega)^2\cdot\alpha}\cdot\left(\frac{u_V}{2\alpha}\right)^2\cdot e^{+i2\omega t}-e^{\beta\cdot t}\cdot\frac{1}{(\beta-i\omega)^2\cdot\alpha}\cdot\left(\frac{u_V}{2\alpha}\right)^2\cdot e^{-i2\omega t} \qquad \text{Eq. SM37}$$

By re-grouping the corresponding terms:

$$\frac{d\varphi_1(t)}{dt}\approx-\frac{u_0\cdot u_v\cdot\left(1-\frac{1}{\alpha\beta}\right)}{2i\cdot\alpha^2(\beta+i\omega)}\cdot e^{(\beta+i\omega)t}+\frac{u_0\cdot u_v\cdot\left(1-\frac{1}{\alpha\beta}\right)}{2i\cdot\alpha^2(\beta-i\omega)}\cdot e^{(\beta-i\omega)t}+\left(\frac{u_V}{2\alpha}\right)^2\cdot\frac{1}{\beta+i\omega}\left(1-\frac{1}{(\beta+i\omega)\cdot\alpha}\right)\cdot e^{(\beta+i2\omega)t}+\left(\frac{u_V}{2\alpha}\right)^2\cdot\frac{1}{\beta-i\omega}\cdot\left(1-\frac{1}{(\beta-i\omega)\cdot\alpha}\right)\cdot e^{(\beta-i2\omega)t}. \qquad \text{Eq.SM38}$$

The Eq. SM38 is easy to integrate:

$$\varphi_1(t) \approx \varphi_{10} - \frac{u_0 \cdot u_v \cdot \left(1-\frac{1}{\alpha\beta}\right)}{2i \cdot \alpha^2 (\beta+i\omega)^2} \cdot e^{(\beta+i\omega)t} + \frac{u_0 \cdot u_v \cdot \left(1-\frac{1}{\alpha\beta}\right)}{2i \cdot \alpha^2 (\beta-i\omega)^2} \cdot e^{(\beta-i\omega)t} + \left(\frac{u_V}{2\alpha}\right)^2 \cdot \frac{1}{\beta+i\omega} \cdot \frac{1}{\beta+i2\omega} \cdot \left(1 - \frac{1}{(\beta+i\omega)\cdot\alpha}\right) \cdot e^{(\beta+i2\omega)t} + \left(\frac{u_V}{2\alpha}\right)^2 \cdot \frac{1}{\beta-i\omega} \cdot \frac{1}{\beta-i2\omega} \cdot \left(1 - \frac{1}{(\beta-i\omega)\cdot\alpha}\right) \cdot e^{(\beta-i2\omega)t}. \qquad \text{Eq. SM39}$$

With $\Phi_1(t) = \varphi_1(t) \cdot e^{-\beta \cdot t}$, one obtains:

$$\Phi_1(t) \approx \varphi_{10} \cdot e^{-\beta \cdot t} - i \cdot \frac{u_V \cdot u_0 \cdot \left(1-\frac{1}{\alpha\beta}\right)}{2\alpha^2 \cdot [(\beta^2-\omega^2)^2 + 4 \cdot \beta^2 \cdot \omega^2]} \cdot \left[\left[\left(\beta^2 - \omega^2\right) - i(2 \cdot \beta \cdot \omega)\right] \cdot e^{i\omega t} - \left[\left(\beta^2 - \omega^2\right) + i(2 \cdot \beta \cdot \omega)\right] \cdot e^{-i\omega t}\right] + \frac{u_V{}^2}{4 \cdot \alpha^3 \cdot (\beta^2 + 4 \cdot \omega^2) \cdot [(\beta^2-\omega^2)^2 + 4 \cdot \beta^2 \cdot \omega^2]} \cdot \left[\left[(\alpha \cdot \beta - 1) + i \cdot \alpha \cdot \omega\right] \cdot \left[\left(\beta^2 - \omega^2\right) - \beta \cdot i2 \cdot \omega\right] \cdot (\beta - i2\omega) \cdot e^{i2\omega t} + \left[(\alpha \cdot \beta - 1) + i \cdot \alpha \cdot \omega\right] \cdot \left[\left(\beta^2 - \omega^2\right) + \beta \cdot i2 \cdot \omega\right] \cdot (\beta + i2\omega) \cdot e^{i2\omega t}\right] \qquad \text{Eq. SM40}$$

and for the stationary oscillations in the long-time limit ($t \gg 1/\beta$):

$$\Phi_1(t) \approx \varphi_{10} \cdot e^{-\beta \cdot t} - i \cdot \frac{u_V \cdot u_0 \cdot \left(1-\frac{1}{\alpha\beta}\right)}{2\alpha^2 \cdot [(\beta^2-\omega^2)^2 + 4 \cdot \beta^2 \cdot \omega^2]} \cdot \left[\left[\left(\beta^2 - \omega^2\right) - i(2 \cdot \beta \cdot \omega)\right] \cdot e^{i\omega t} - \left[\left(\beta^2 - \omega^2\right) + i(2 \cdot \beta \cdot \omega)\right] \cdot e^{-i\omega t}\right] + \frac{u_V{}^2}{4 \cdot \alpha^3 \cdot (\beta^2 + 4 \cdot \omega^2) \cdot [(\beta^2-\omega^2)^2 + 4 \cdot \beta^2 \cdot \omega^2]} \cdot \left[\left[(\alpha \cdot \beta - 1) + i \cdot \alpha \cdot \omega\right] \cdot \left[\left(\beta^2 - \omega^2\right) - \beta \cdot i2 \cdot \omega\right] \cdot (\beta - i2\omega) \cdot e^{i2\omega t} + \left[(\alpha \cdot \beta - 1) + i \cdot \alpha \cdot \omega\right] \cdot \left[\left(\beta^2 - \omega^2\right) + \beta \cdot i2 \cdot \omega\right] \cdot (\beta + i2\omega) \cdot e^{i2\omega t}\right]. \qquad \text{Eq. SM41}$$

The Eq. SM41 can be rearranged into several equivalent forms that, however, always suggest components that are modulated by fundamental frequency of the light modulation ωt and first upper harmonic modulation of $2\omega t$. For Discussion, see the SUMMARY above.

References

Debye P. (1913) Ver. Deut. Phys. Gesell. 15, 777

James F.A.J.L., ed. (1996) The Correspondence of Micheal Faraday, Volume 3, 1841-1848, Letter 1674, pp. 317-318. The Institution of Electrical Engineering and Technology, London, United Kingdom

Lazár D. (2009) Modelling of light-induced chlorophyll *a* fluorescence rise (O-J-I-P transient) and changes in 820 nm-transmittance signal of photosynthesis. Photosynthetica 47, 483-498

Nedbal L., Březina V. (2002) Complex metabolic oscillations in plants forced by harmonic irradiance. Biophysical Journal 83, 2180-2189

Nedbal L., Březina V., Adamec F., Štys D., Oja V, Laisk A., Govindjee (2003) Negative feedback regulation is responsible for the non-linear modulation of photosynthetic activity in plants and cyanobacteria exposed to a dynamic light environment. Biochimica et Biophysica Acta -Bioenergetics 1607, 5-17

Nedbal L., Březina V., Červený J., Trtílek M. (2005) Photosynthesis in dynamic light: systems biology of unconventional chlorophyll fluorescence transients in *Synechocystis* sp. PCC 6803. Photosynthesis Research 84, 99-106

Schwartz L. (2008) Mathematics for the physical sciences. Courier Dover Publications

von Bertalanffy L. (1993) General system theory: Foundations, development, applications. Georges Braziller, Inc., 1993.